Laser-Processed Nanosilicon: A Multifunctional Nanomaterial for Energy and Healthcare

Andrei Kabashin, Ajay Singh, Mark Swihart, Irina Zavestovskaya, Paras Prasad

Review

Laser Processed Nanosilicon: A Multifunctional Nanomaterial for Energy and Health Care

Andrei V. Kabashin, Ajay Singh, Mark T. Swihart, Irina N. Zavestovskaya, and Paras N. Prasad

ACS Nano, **Just Accepted Manuscript** • DOI: 10.1021/acsnano.9b04610 • Publication Date (Web): 06 Sep 2019

Laser Processed Nanosilicon: A Multifunctional Nanomaterial for Energy and Health Care

Andrei V. Kabashin,[†,‡] Ajay Singh,[§] Mark T. Swihart,[§,∥] Irina N. Zavestovskaya,[‡] and Paras N. Prasad[§,‡]

[†]Aix-Marseille Univ, CNRS, LP3, Marseille, France

[‡]MEPhI, Institute of Engineering Physics for Biomedicine (PhysBio), 31 Kashirskoe sh., 115409 Moscow, Russia

[§]Institute for Lasers, Photonics, and Biophotonics, The University at Buffalo, The State University of New York, Buffalo, New York, 14260-3000, USA

[∥]Department of Chemical and Biological Engineering and RENEW Institute, The University at Buffalo, The State University of New York, Buffalo, New York, 14260-4200, USA

Abstract: This review describes promising laser-based approaches to produce silicon nanostructures, including laser ablation of solid Si targets in residual gases and liquids and laser pyrolysis of silane. These methods are different from, and complementary to, widely used porous silicon technology and alternative synthesis routes. One can use these methods to make stable colloidal dispersions of silicon nanoparticles in both organic and aqueous media, which are suitable for a multitude of applications across the important fields of energy and health care. Size tailoring allows production of Si quantum dots with efficient photoluminescence that can be tuned across a broad spectral range from the visible to near-IR by varying particle size and surface

functionalization. These nanoparticles can also be integrated with other nanomaterials to make multifunctional composites incorporating magnetic and/or plasmonic components. In the energy domain, this review highlights applications to photovoltaics and photodetectors, nanostructured silicon anodes for lithium ion batteries, and hydrogen generation from water. Application to nanobiophotonics and nanomedicine profit from the excellent biocompatibility and biodegradability of nanosilicon. These applications encompass several types of bioimaging and various therapies, including photodynamic therapy (PDT), RF thermal therapy, and radiotherapy. The review concludes with a discussion of challenges and opportunities in the applications of laser-processed nanosilicon.

Keywords: nanosilicon, silicon nanoparticles, silicon quantum dots, nanosilicon for energy, pulsed laser ablation, pulsed laser ablation in liquids (PLAL), laser pyrolysis, nanobiophotonics, and nanomedicine

Vocabulary:

Pulsed laser ablation: a physical vapor deposition technique in which a high-power pulsed laser beam is focus on a target material that is to be deposited as a thin film on a substrate in vacuum, or converted into nanoparticles in a low-pressure background gas.

Pulsed laser ablation in liquid (PLAL): a method in which a high-power pulsed laser beam is used to vaporize material from a solid target in a liquid environment to directly produce colloidally-dispersed nanoparticles.

Laser pyrolysis: a method of preparing nanoparticles *via* laser-induced heating of a gas-phase precursor mixture. Laser heating allows very rapid initiation and quenching of particle formation, producing nanocrystals of more uniform size compared to other gas-phase methods of nanoparticle synthesis.

Silicon quantum dot: a crystalline silicon nanoparticle with diameter significantly less than twice the Bohr exciton radius in silicon (~4.5 nm) such that size-dependent properties emerge due to quantum confinement effects.

Nanophotonics: the study and application of the interaction of nano-scale objects, with light and the behavior of light at nanometer scales.

Bionanophotonics: the application of nanophotonics to biological and medical research and applications.

Nanomedicine: the application of nanotechnology, including nanoscale materials and phenomena specifically occurring at the nanoscale, to medical diagnostics and therapy.

Silicon (Si), which makes up 28% of the mass of the Earth's crust, has a variety of useful properties and can be refined by relatively inexpensive methods. Si is best known for its outstanding semiconductor properties, as its conductivity can be controlled through addition of small concentrations of doping elements (typically, boron and phosphorus). On this basis, Si has become the core material of modern electronics, from which a plethora of devices, such as transistors, solar cells, and photodetectors for computers, television, smart phones and other applications, are created.[1] On the other hand, being present as orthosilicate (SiO_4^{4-}) in many tissues, silicon (Si) is an essential element in living organisms.[2-4] This abundance in nature and presence in living systems are the basis for the excellent compatibility of Si and silicon-containing compounds with biological systems. Furthermore, elemental Si is biodegradable and safely excreted from the body,[5, 6] which is a rather unusual feature for inorganic elements, making it promising for biomedical applications.

Even more astonishing properties of silicon become possible upon decreasing the Si crystal size down to the nanoscale. Due to significant modification of electronic energy bands[7] and other phenomena, nanostructured Si (nanosilicon) can become strongly luminescent in the visible and near infrared,[8, 9] although bulk crystalline Si has only a small (1.11 eV at room temperature) and indirect band gap. These luminescent properties of nanosilicon open up many opportunities for optoelectronic applications[10] and for the development of fluorophores and contrast agents for bioimaging.[11-13] On the other hand, nanosilicon structures can exhibit dramatically increased absorption of light in the ultraviolet, visible and infrared,[14-16] which promises attractive applications in photodetectors, image sensors, thermal imaging cameras, and solar panels. In addition, Si nanostructures can provide much-improved characteristics as anode materials in lithium-ion batteries compared to conventional microparticle counterparts[17-20] and, due to a large

highly-active surface area, can be used for hydrogen generation from water to power fuel cells.[21-23] Nanosilicon can finally enable a variety of therapeutic modalities, including drug vectoring,[24, 25] photodynamic therapy,[26-28] and infrared,[29] radio frequency,[30] and ultrasound-induced[31] hyperthermia for cancer treatment.

The diverse array of possible nanosilicon applications necessitates the choice of the most suitable methods for its synthesis for each application. Most of these applications require the fabrication of luminescent silicon nanostructures with emission at a particular wavelength in blue, green or red-infrared range.[8, 9] In addition, optoelectronic, photovoltaic, image sensor, and solar panel applications may require "dry" fabrication routes that could be compatible with Si processing technology for further integration of functional devices into standard microelectronic chips/platforms.[1] On the other hand, biomedical applications typically require luminescence emission in the window of relative tissue transparency, *i.e.*, the near-infrared range (650-850 nm). These applications also require water-dispersibility and purity of nanosilicon.[32-34]. Methods for the fabrication of silicon can be divided into chemical, physical, physicochemical, and electrochemical. Wet chemical synthesis routes, including solution-phase reduction,[35-37] microemulsion techniques,[38, 39] supercritical fluid synthesis,[40] solid-state disproportionation,[41, 42] microwave synthesis,[43, 44] sonochemical synthesis,[45] and mechano-chemical synthesis,[46] have been reported for producing luminescent Si nanocrystals. However, many of these methods use toxic substances (*e.g.*, organosilicon precursors, reducing agents, or etching agents) whose residual presence in the product can complicate biomedical applications. Some of these methods may not be reproducible in other labs, may not actually produce fully reduced and crystalline silicon, or may produce silicon by routes other than those proposed in the original publications. Our purpose here is not to critically evaluate each of these reports, but simply to provide an entry into the diverse

literature on non-laser-based nanosilicon fabrication methods. Dry fabrication methods such as thermal annealing of SiO_x polymers,[47, 48] slow combustion,[49, 50] thermal decomposition,[51] microwave plasma,[9, 52] low-pressure non-thermal plasma,[53-55] gas-evaporation,[56] and chemical vapor deposition (CVD)[57, 58] are also efficient for fabricating luminescent Si crystals and more compatible with silicon processing technology, but they typically require additional chemical processing steps to separate and water-disperse crystals and stabilize luminescence emission in solutions.[59] Porous silicon technology based on electrochemical etching of silicon is the most popular approach to fabricate luminescent Si crystals, and has been used in more than 80-85% of studies.[8, 33, 34] Formed originally on a silicon wafer, porous silicon crystals can later be milled, dispersed in aqueous solutions and employed in biological applications, *e.g.,* as markers in bioimaging.[33, 34] However, so formed nanostructures may have a wide dispersion of both size and shape of crystals, and may be contaminated by hydrofluoric acid derivatives,[60] which is not desirable for many applications. In addition, wet porous silicon synthesis is not well compatible with silicon microelectronics technology, which complicates many applications that require the integration of porous silicon structures into microelectronics platforms. Spectral position and efficiency of luminescence are considered key parameters for the majority of projected applications. These parameters are determined by the luminescence mechanisms and depend on both the methods of nanocrystal preparation and surface conditioning.[61-65]. Silicon nanoparticles (NPs) produced by wet chemical methods typically have a low crystallinity and most commonly emit blue photoluminescence,[66] which is typically attributed to defect states,[67, 68] although luminescence emission can be modified and shifted toward the green or red range by appropriate surface engineering. Dasog *et al.*[69] demonstrated the important role of trace nitrogen, as well as oxygen, in producing blue luminescence from silicon nanocrystals of high apparent crystallinity.

In contrast, porous silicon technology[8, 33, 34] and high temperature routes[40, 41, 53-55] can produce material with higher crystallinity and high purity, which is capable of generating size-tunable photoluminescence associated with emission from quantum-confined excitonic states in ultrasmall crystalline silicon cores.[70-72]

A series of studies over the years have shown that many problems in applications of nanosilicon can be solved using laser processing-based fabrication routes. Laser radiation can be delivered through gaseous or liquid media (inert or reactive) and be focused to cause ablation of material from a Si target[73] or initiate decomposition and particle-forming chemical reactions in Si-containing gases (*e.g.*, silane, SiH_4).[74, 75] Through these processing routes, one can synthesize high quality nanosilicon crystals in the form of nanostructured films, nanopowders, and colloidal dispersions. Some laser-based synthesis methods, particularly pulsed laser ablation in liquid, can produce stable aqueous dispersions in a single step, [73, 76] while others, such as gas-phase laser pyrolysis, are similar to other dry synthesis methods with respect to the required post-processing steps.[77, 78] Moreover, laser processing enables one to fabricate contamination-free nanosilicon structures when performed in clean conditions (deionized water, non-toxic gases). This review article aims to provide an overview of laser processing methods for the fabrication of nanosilicon and describes possible uses of these nanosilicon materials in energy and health care applications.

Laser Fabrication of Nanosilicon

Laser-ablative Synthesis

Laser ablation has proved its high efficiency in producing a variety of nanostructured materials, including silicon-based ones.[73] The action of intense laser radiation on a solid Si target can ablate the target material leading to the production of periodic micro- and

nanoarchitectures on the surface.[15, 16, 79] Furthermore, material is typically ablated in the form of atoms and nanoclusters,[80-82] which then experience condensation in the vapor phase upon interaction with their environment, to form larger clusters. When produced in a gaseous/vacuum ambient, these nanoclusters can then be crystallized on a substrate to form a nanostructured film or a powder-like deposit. When produced in a liquid ambient, the nanoclusters can form a colloidal nanoparticle dispersion. Notably, nanostructures formed by laser ablation in both media can exhibit very promising properties for a variety of applications.

Pulsed laser ablation in gaseous environment. The straightforward configuration is based on a conventional Pulsed Laser Deposition (PLD) geometry, which does not imply any synthetic selection of ablated nanoclusters. A typical PLD geometry is shown in Figure 1. Here, radiation from a nanosecond laser with an intensity of 10^8 - 10^9 W/cm^2 is focused on a rotating Si target at an inclined angle of incidence (~ 45°). The intense radiation causes ablation of the material and formation of a plasma plume that expands perpendicular to the target surface. Such experiments are normally performed using UV radiation from excimer lasers (248 nm from KrF or 193 nm from ArF), which is transmitted through the plasma plume. This enables one to minimize losses of radiation energy before reaching the target and allows rapid cooling of ablated clusters. A substrate is typically installed at some distance (generally 2-3 cm) from the target. The ablation can be performed either in vacuum or in a residual gas. When the ablation is performed at a relatively low gas pressure (< 10^{-2} Torr), the growth of nanoclusters is hardly controllable and they typically arrive to the substrate as-ablated and crystalize directly on its surface, forming mostly amorphous film with minimal porosity.[83-86] In contrast, laser ablation in an inert residual gas (He, Ar) at a

moderate pressure of 0.1-10 Torr allows a degree of control of the characteristics of the product nanostructures.[83-94] In this case, gas atoms (or molecules) and their ionized species serve to control the growth and crystallization of nanoclusters during their collisions.[80-82]

As shown in Figure 1b, laser-ablated Si nanoclusters are typically 2-4 nm in diameter, while high resolution TEM images reveal that the nanoclusters can be highly crystalline (Figure 1c). The deposition of these gas suspended nanoclusters on a substrate facing the target leads to the formation of a thin nanostructured Si-based film. When relatively thick (several

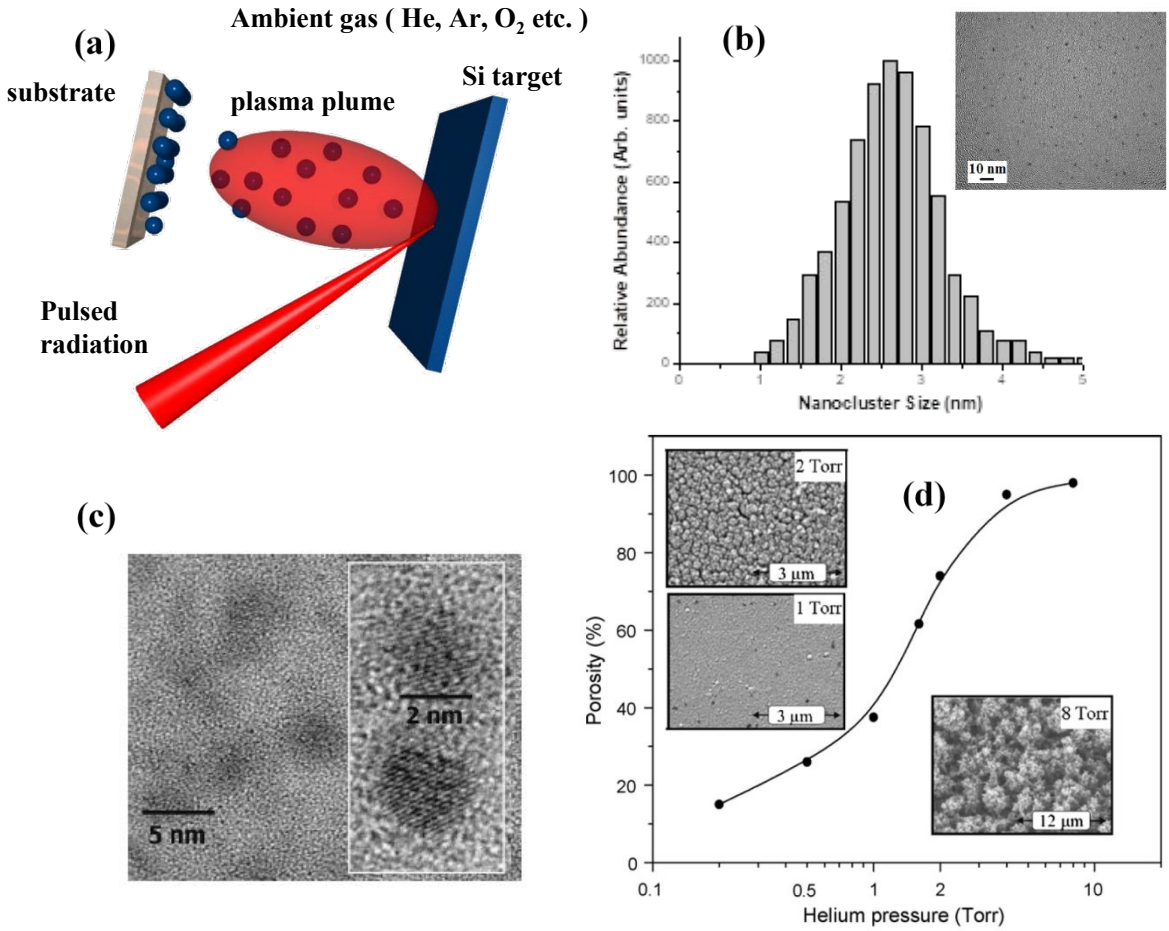

Figure 1. *(a) Schematic of PLD experiment for deposition of Si-based nanostructured films; (b) Transmission Electron Microscopy (TEM) image of laser-ablated Si nanoclusters and corresponding nanocluster size distribution (Adapted from Ref. 93 with permission from AIP Publishing); (c) High resolution TEM images of as-deposited Si particles (Adapted from Ref. 94 with permission from Elsevier). (d) Dependence of film porosity on helium pressure during the deposition. Insets show morphologies of the films formed under different gas pressures (Adapted from Ref. 93 with permission from AIP Publishing).*

hundreds of nm or more), the films can be multi-colored due to thin film interference effects. The presence of ambient neutral gas was shown to be the key parameter, which determines the properties of the formed Si crystals, as this parameter can affect both the size[81, 82] and the morphology of deposited films. As shown in Figure 1d, increasing the He pressure during ablation of a Si target leads to a gradual increase of film porosity. While the ablation at low pressures (<0.5 Torr) leads to the formation of dense films with porosities lower than 25%, increasing the background pressure leads to a gradual increase of porosity to more than 90%. Ablation at high pressures (5-10 Torr) leads to the deposition of web-like powders with extremely weak adhesion to the substrate.[93] Such a strong dependence of morphology on ambient gas pressure was explained by enhanced cooling of nanoclusters due to an increased number of collisions with He atoms and their crystallization before reaching the substrate.[93]

The focus of early studies was mainly concentrated on the formation of Si-based nanostructures, which could provide substantial photoluminescence (PL)[83-90] and electroluminescence (EL),[95] especially in the blue spectral region. In contrast to "wet" chemistry-produced porous silicon, the films fabricated by "dry" laser-ablative synthesis were expected to have excellent compatibility with the Si microelectronic processing technology, which would facilitate the implementation of Si-based optoelectronic emitters and other devices. Indeed, laser-synthesized nanostructured films have been observed to exhibit PL with quantum yields reaching several percent, but reported PL properties were rather contradictory. Several groups tried to establish a correlation between the spectral positions of PL peaks and the size of formed nanostructures, and obtained some interesting data. As an example, by changing the laser pulse fluence during ablation, Patrone[88]

managed to obtain size-dependent PL spectra (Figure 2a). In contrast, Makimura[85, 86] and Yoshida[84, 87, 90] recorded three fixed PL peaks at 1.5-1.75 eV, 2.2-2.3 eV and 2.7-2.8 eV from films prepared under similar conditions (Figure 2b). On the other hand, Yoshida[95, 96] demonstrated efficient electroluminescence from laser-ablated films, and the observed 1.66 eV emission matched one of the PL peaks. Later, Kabashin[93] showed that conditions for producing size-dependent or fixed PL bands can be reached using different ambient pressures of He during the deposition, leading to different porosities of the formed films (Figure 1d). Low porosity films deposited under relatively low pressures could indeed exhibit tunable PL spectra that red-shifted with increasing nanoparticle size, but the intensities of these emissions were much weaker. This spectrally tuned emission can be due to quantum confinement effects, but other mechanisms cannot be ruled out, taking into account rather different manifestation of properties of quantum confinement effects recorded in the case of porous silicon.[32-34] Highly porous films formed at P > 1.5 Torr provided 1-2 orders stronger signals, presenting two fixed bands (1.5-1.75 eV and 2.2-2.3 eV), similar to the ones observed by other groups[84-87] (the third band around 2.7 eV could

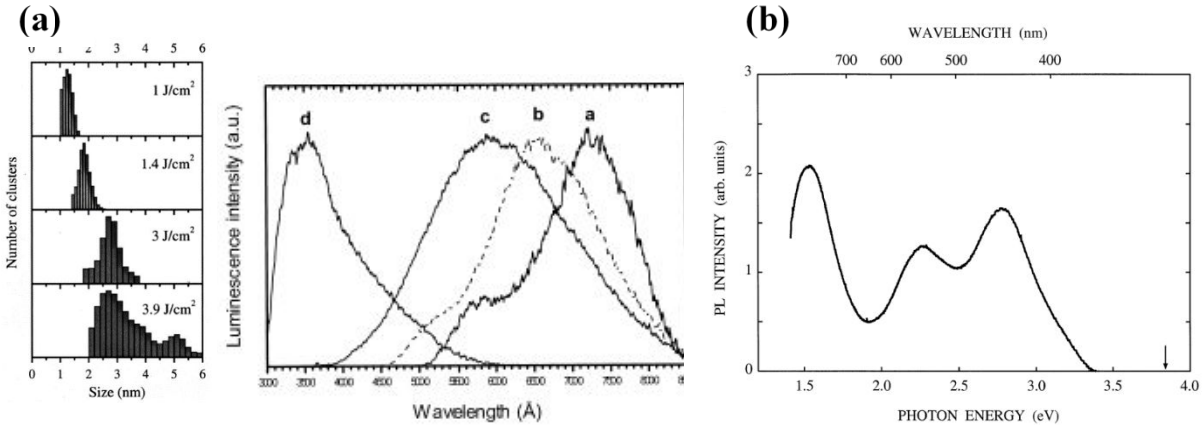

Figure 2. *(a) Nanoparticle size distributions and PL spectra of nanosilicon films produced using different laser fluences: 3.9 J/cm²- a; 3 J/cm² – b; 1.4 J/cm² – c; 1 J/cm² –d. Adapted from Ref. 88 with permission from AIP Publishing; (b) PL spectrum of Si nanocrystal-based film synthesized by laser ablation in residual He and then annealed in Ar (1000 C, 30 min). The data were taken from Ref. 86 with permission from Elsevier.*

not be observed due to overlap with the 488 nm excitation wavelength). The generation of two fixed bands with much enhanced intensity could be related to both better crystal quality as a result of nanocluster crystallization in the vapor phase (before reaching the substrate) and better conditions for oxidation of inner layers of porous films to passivate the crystals in order to remove non-radiative centers.[97]

Based on the similarity of PL bands for alternative nanosilicon structures, the origin of 2.2-2.3 and 2.7-2.8 eV emissions can be assigned to defects in SiO_x structures,[32, 34, 67, 68] while the origin of 1.5-1.75 eV (640-800 nm) emission can be attributed to quantum-confined excitonic states in Si nanocrystals.[32-34, 70-72] The defect- and quantum confinement mechanisms of 2.7-2.8 and 1.5-1.75 eV emissions were confirmed by their characteristic PL time decays, having ns and μs scales, respectively (Figure 3b). In the case of porous silicon, the generation of the 1.5-1.75 eV excitonic band becomes possible due to a hydrogenation step that involves exposing the Si surface to solutions of HF or a mixture of HF and HNO_3, followed by natural oxidation in air or ethanol, to provide hydroxyl-based passivation of the surface and the removal of non-radiative recombination centers.[32, 34, 97]

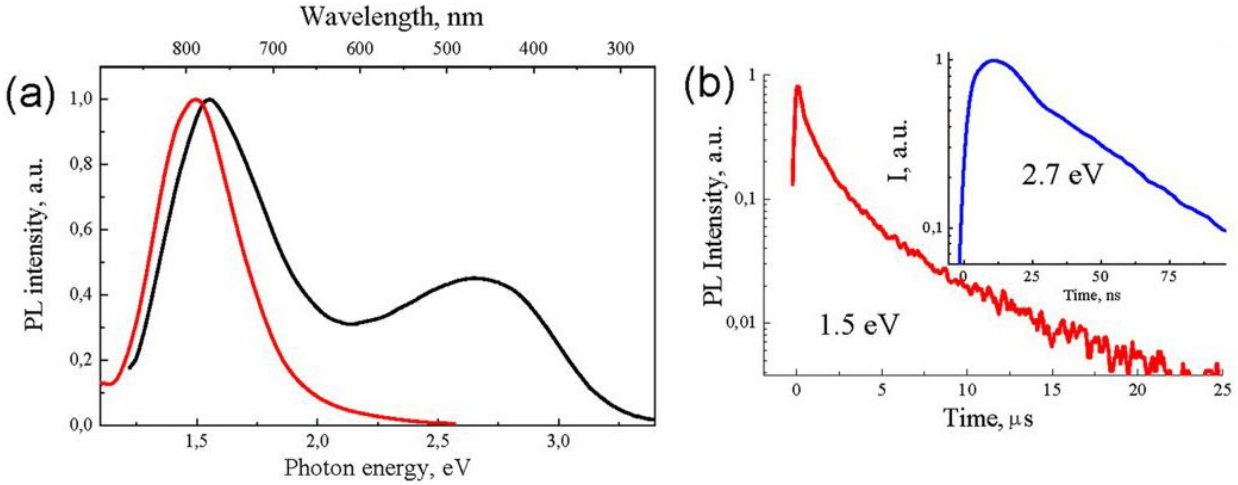

Figure 3. *(a) PL spectra of nanosilicon films synthesized by PLD (red curve) and aqueous dispersions of Si nanoparticles obtained by milling of these films by ultrasound (black curve); (b) Transient PL signal for 1.5 eV exciton band and 2.7 eV defect-related band (inset). Adapted from Ref. 13 with permission under a Creative Commons CC-BY license.*

In contrast, in the case of laser-synthesized nanostructures, the exciton-based PL emission was recorded despite the absence of such a hydrogenation step. Gongalsky[13] later explained the recorded emission by specific conditions of nanocluster growth in the plasma plume (involving rapid heating and cooling stages). Laser-ablated nanoclusters move through a long-living plasma plume, which contains He ions and hot electrons having a significant excess of energy (tens of eV).[81, 82] Since electron-ion recombination events can increase temperature of small nanoclusters up to 1000 K,[98] laser-ablated nanoclusters are expected to be strongly heated before reaching the substrate. A subsequent cooling of nanoclusters *via* their collisions with He atoms outside the hot plume conditions the production of nearly perfect low-defect Si quantum dots. Such nanocrystals start to exhibit exciton PL just after their exposure to ambient air, with gradually increasing intensity during the first 2-4 weeks of their aging under these conditions. Such purely oxygen-related passivation of the Si crystal surface appears to be very efficient when high quality crystals are formed *via* PLD.

Gongalsky[13] also showed that Si nanocrystals can be efficiently removed from the substrate and milled using ultrasound, to form separated nanoparticles that can be easily dispersed in water or physiological solutions. Notably, the PL emission of the exciton band remained significant, even after dispersion of these nanoparticles in aqueous solutions (Figure 3a), which suggests their potential use as markers for bioimaging. A huge advantage of these markers is that their emission lies in the window of relative tissue transparency (700-1000 nm). The very long time decay (μs) of their emission (Figure 3b) renders possible an easy removal of background biological autofluorescence (with ns time decay) using time gating techniques like those demonstrated by Gu *et al.*[12].

Additional size control of laser-synthesized Si nanoparticles can be achieved by the application of size-selective synthetic routes. Several studies have used external control of plume dynamics and cluster size selection. As an example, El-Shall introduced the laser vaporization-controlled condensation method, in which an external gradient of temperature was applied to control the plasma plume evolution. Despite better control of structural characteristics of deposited films, their photoluminescent properties were similar to those of films prepared by conventional PLD. Seto[99, 100] achieved a narrow size distribution of laser-synthesized silicon nanoclusters by applying a differential mobility analyzer (DMA). Here, laser-synthesized nanoclusters were transported by a helium gas stream and then size-classified in the gas phase using the DMA. Nanostructured films prepared by such a size-selection method exhibited sharp size-dependent PL spectra with the peak shifting from 1.34 eV to 1.79 eV with decreasing nanocrystal size from 4.9 nm down to 2.1 nm (Figure 4). The latter results are of importance for optoelectronics applications.

A series of studies were devoted to laser-ablative fabrication of Si-based nanowires with great potential in applications including nanoelectronics, optoelectronics, and solar cells. Here, most approaches have been based on the use of metal (Fe, Ni, Au, *etc.*) catalysts, which enable the formation of anisotropic Si-based structures under high temperature conditions.[101-104] In a common configuration, a metal-doped Si (or Si + SiO_2) target is placed in a quartz tube within a furnace maintained at high temperature (100-1200 °C). A water-cooled finger is inserted to the furnace to collect product nanostructures, while Ar gas flows through the chamber, and vacuum is created by pumping. Radiation from an ultraviolet excimer laser (248 nm) is used to ablate the target, while the material is collected on the finger surface. Such a configuration enables one to fabricate a variety of nanowire architectures having diameters of 15-20 nm and consisting of a silicon crystalline core covered by a silicon dioxide shell.

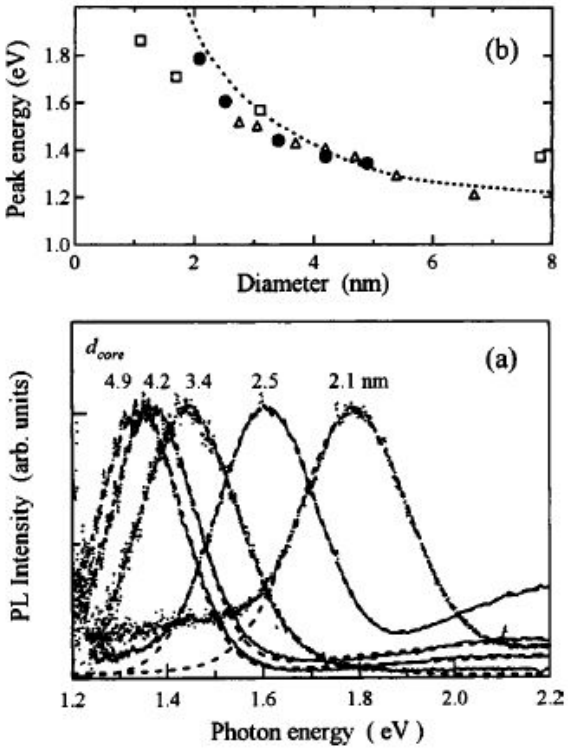

Figure 4. *(a) PL spectra of nanosilicon films for different mean crystal sizes. (b) Dependence of PL peak energy on Si crystal size. Adapted from Ref. 100 with permission from AIP Publishing.*

More recently, interest in the fabrication of relatively large spherical Si nanoparticles (100-400 nm) and arrays of these particles on a substrate has grown rapidly. Interest in these structures arises from a series of recently-discovered effects associated with the excitation of optical magnetic and optical electric dipole resonances within dielectric spheres.[105-109] Such resonances are somewhat similar to split ring resonators, but they have much smaller losses and are able to shift the spectral position of the magnetic resonance into the visible range. Because the excitation of such resonances requires relatively high refractive index of a nanoparticle material, silicon with its refractive index exceeding 3.5 is one of the best candidates. Laser ablation in gaseous ambient was shown to enable the fabrication of large Si-based nanoparticles of the required quality. Here, methods of femtosecond laser ablation in air appeared to be most effective for obtaining the desired characteristics. In one geometry, the material was ablated from a Si wafer by laser radiation (800

nm, 100 fs) and then redeposited on the same substrate, leading to the formation of Si nanoparticles with sizes ranging from several tens of nm to 200 nm.[107] In another geometry of light-induced forward transfer (LIFT), fs radiation (120 fs, 800 nm) was transmitted through a transparent glass substrate and then used for the ablation of material from a bulk Si wafer placed at a small distance from the substrate.[106] Due to the specific hydrodynamics of LIFT, the ablated material was transferred to the substrate, forming spherical nanoparticles with sizes from several tens to several hundreds of nm. We note that the second approach appears preferable, as dielectric resonances can be more easily observed and investigated when the nanoparticles are deposited on a transparent substrate. However, in both geometries, controlling the size and shape distributions of the Si nanostructures was difficult. As one solution to this problem, a ring-shaped distribution of intensity on a Si wafer surface was used under LIFT, and this approach made possible the production of large (> 400 nm) nanoparticles.[110] Later, Chichkov and his colleagues proposed an important modification of the LIFT technique to solve the problem of nanoparticle size control.[109] Here, instead of a bulk Si target, they used a silicon-on-insulator wafer, consisting of an upper crystalline silicon layer (100 nm) deposited on a 200 nm silicon dioxide layer grown on a bulk Si wafer. When such a structure was illuminated by a tightly focused fs beam, the upper Si layer was rapidly heated and melted, while the SiO_2 layer remained unaffected. Under appropriate radiation intensity, increased surface tension led to the formation of a droplet, which moved toward the substrate placed at some distance (5 μm) from the target where it solidified. Using this approach, the authors were able to produce amorphous Si nanoparticles with controllable sizes ranging from tens of nm to hundreds of nm. As a next step, the nanoparticles were fully crystallized by applying a second laser pulse of appropriate duration and intensity.[109] Thus, the LIFT geometry enables one to easily

obtain Si nanoparticle arrays exhibiting dielectric resonances, while the position of these resonances can be tuned by changing conditions of LIFT experiment.

Laser spark processing (LSP). LSP is an alternative method for material nanostructuring in the gaseous phase, which implies the production of a hot plasma in order to modify material properties.[111-114] LSP typically requires infrared laser radiation like that of a pulsed CO_2 laser (10.6 μm wavelength, 1 μs pulse), which is strongly absorbed by the laser-induced plasma itself *via* inverse Bremsstrahlung mechanism.[115] When focused in air or other atmospheric pressure gas, such radiation can initiate a gas breakdown avalanche, which emerges as a bright flash (laser spark) moving toward the focusing lens (Figure 5a). The placement of a target near the lens can lower the breakdown threshold by 2-3 orders of magnitude by providing initial avalanche-triggering electrons.[116] Because almost all radiation energy is absorbed in the front of the plasma shock wave moving toward the lens, a laser spark plasma can accumulate a huge amount of energy. Therefore, nanoclusters ablated from the target by LSP find themselves in a hot plasma with temperatures higher than 10^4 K[115] and intense electromagnetic fields,[117-119] which can lead to modification of their properties. The clusters then return to the focal spot due to hydrodynamic processes in the laser plasma[115] to form a crystalline nanostructured film.

After multi-pulse treatment by LSP in air or other atmospheric pressure gases (Ar, N_2, *etc.*), the Si surface presents an eroded area covered by redeposited nanostructured material with the absence of any notable crater.[113] Note that the morphology of a Si surface, subjected to multi-pulse treatment by conventional ultraviolet or visible laser radiation, is characterized by the formation of characteristic deep craters with microspike structures on the bottom encircled by a "hill" of redeposited material.[113] SEM studies reveal nanoparticles with sizes

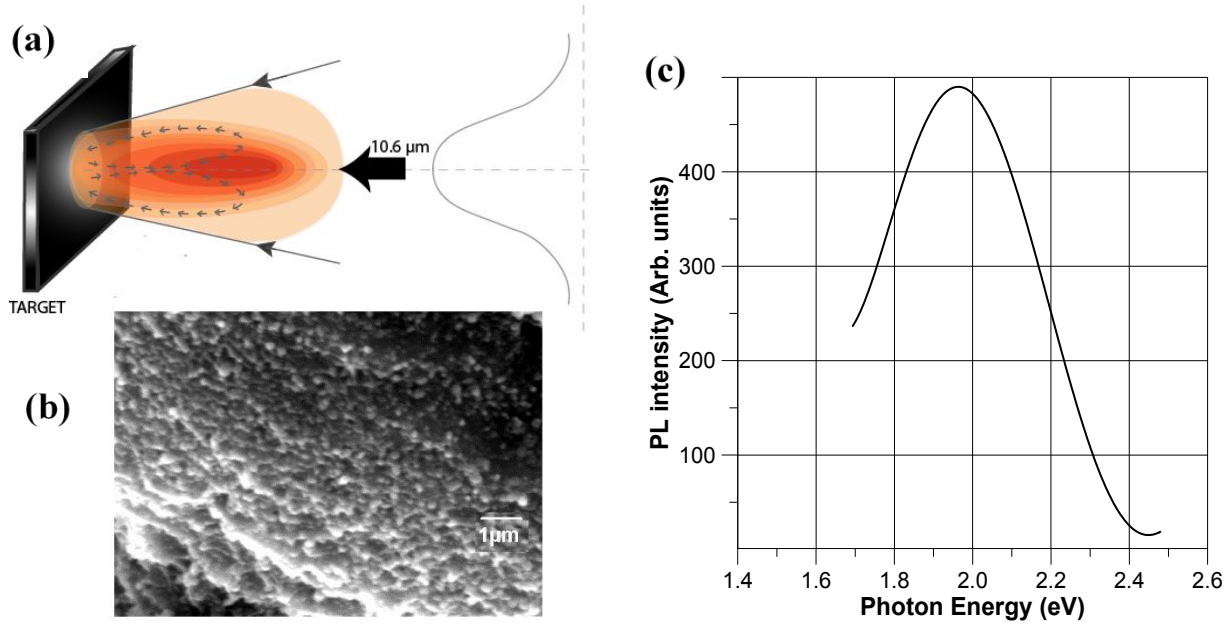

Figure 5. *(a) Schematics of laser-induced air breakdown initiation: A target generates the first electrons, which trigger the avalanche discharge of cold gas molecules. The discharge moves toward the focusing lens absorbing most of the incident radiation power in the plasma forefront. The plasma-based mechanism of radiation power absorption leads to the increase of plasma temperatures up to 10^4-10^5 K; (b) Typical SEM image and (c) PL spectrum from Si nanostructures formed by laser spark processing. PL was excited by 488 nm pumping. Adapted from Ref. 112, 113 with permission from AIP Publishing and Elsevier, respectively.*

ranging from 20 to 70 nm, which are densely packed to form a nanostructured film (Figure 5b). Increasing the laser energy igniting the spark can also lead to formation of microscale flower-like structures associated with coagulation of nanoparticles. Nevertheless, a detailed analysis of the properties of Si layers by XRD and XPS reveals the presence of 2-5 nm crystals embedded into a SiO_x matrix to form larger nanoscale structures.[112] As shown in Figure 5c, the layers prepared by LSP exhibit strong PL with a characteristic band around 1.9-2.0 eV (640-650 nm) having similar characteristics to layers prepared by PLD. The nanocrystals can be dispersed using ultrasound to form colloidal dispersions and then used in bioimaging or optoelectronics applications.

Pulsed laser ablation in liquids (PLAL). PLAL has appeared as an alternative laser-assisted method to fabricate a variety of colloidal nanoparticles in liquid ambients.[76, 120-123]

PLAL is now experiencing spectacular growth due to its simplicity of synthesis (no vacuum equipment is required) and properties of synthesized nanostructures (*e.g.* high purity, spherical shape, and unusual chemistry).[124] In a common ablation geometry, a solid target immersed in a liquid is ablated by laser radiation, forming nanoclusters, which then coalesce during their cooling in the liquid environment to yield a colloidal nanoparticle dispersion.[73] However, in cases of ablation of Si and other materials by conventional ns lasers (*e.g.* Nd-YAG), size characteristics of the produced nanoparticles are difficult to control. Indeed, a nanosecond laser radiation typically has high energy (mJ/pulse and larger), which leads to the initiation of hot plasma near the target, whose energy is then transferred to the liquid to form a cavitation bubble.[73] Subsequent phenomena associated with target heating by the plasma and the collapse of the cavitation bubble (releasing mechanical energy) inevitably lead to uncontrolled parasitic ablation of the material and the appearance of a second broadly size-dispersed population of nanoparticles, in addition to the first narrow population caused by purely radiative ablation.[123] Therefore, Si nanoparticles prepared under a nanosecond ablation regime, are typically relatively large and broadly size-dispersed.[122, 125-127] As we have shown,[123, 128] the size dispersion problem can be solved by operating in the ultrashort (femtosecond) laser ablation regime, which is characterized by a 10 times lower energy to initiate ablation of material. In this case, ablation under low intensities (near the ablation threshold) minimizes plasma heating and bubble collapse effects, and thus suppresses the formation of the second broadly dispersed population of nanoparticles. An example of Si nanoparticles prepared by fs laser ablation from a Si target near the ablation threshold, is shown in Figure 6.

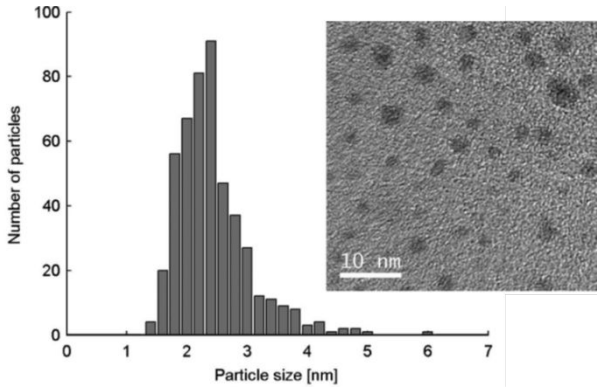

Figure 6. *A TEM image of Si nanoparticles produced by femtosecond laser ablation from a silicon target in deionized water (near-threshold ablation conditions) and corresponding TEM image of formed nanoparticles. Adapted from Ref. 128 with permission under a Creative Commons CC-BY license.*

Laser fragmentation from pre-prepared colloids is another important modification of the PLAL method to improve size and structural characteristics of formed Si nanoparticles. Here, fs laser fragmentation looks especially promising due to advantages offered by the non-linear character of interaction of ultrafast laser radiation with a liquid environment. We have shown that such an interaction leads to the generation of a white light "supercontinuum" of fs duration,[129, 130] which can illuminate the whole liquid volume. As a result, the supercontinuum-based radiation can ablate micro/nano colloids in a large volume, creating identical conditions for re-growth of nanoclusters in order to obtain uniform size characteristics of the formed nanoparticles. In the case of Si, fs laser fragmentation can further be simplified by using a mechanical milling step to prepare initial colloids.[131] Here, a Si wafer is milled to form arbitrarily-shaped particles with characteristic sizes of 0.5-5 μm (Figure 7a). In a second step, the radiation from a fs laser is focused in the very center of a glass vessel filled an aqueous dispersion of Si microparticles, while the solution is constantly mixed by a magnetic stirrer (Figure 7b,c). As shown in Figure 7, such fs laser fragmentation leads to the production of dispersions of low polydispersity Si nanoparticles. The size of these nanoparticles can be varied between a few nm and several

tens of nm by changing the initial concentration of the microcolloid (Figure 7d). As seen in high-resolution TEM and electron-diffraction images (Figure 7e), laser-synthesized nanoparticles possess a crystalline Si core (Figure 7e), while XPS studies reveal the presence of a few nm thick oxide shell on their surface.[131, 132] The number of oxygen-related defects in the Si core can be controlled by varying the oxygen content of the solvent during the ablation process. This can be done by fragmenting Si microcolloids in oxygen-rich conditions (deionized water) or oxygen-free conditions (with O_2 concentration reduced *via* Ar gas bubbling).[132] Although the formed nanoparticles are bare (ligand-free), dispersions of these nanoparticles exhibit very high stability due to a strong negative charge of nanoparticles (exceeding -35 mV according to zeta-potential studies).[131] In contrast to

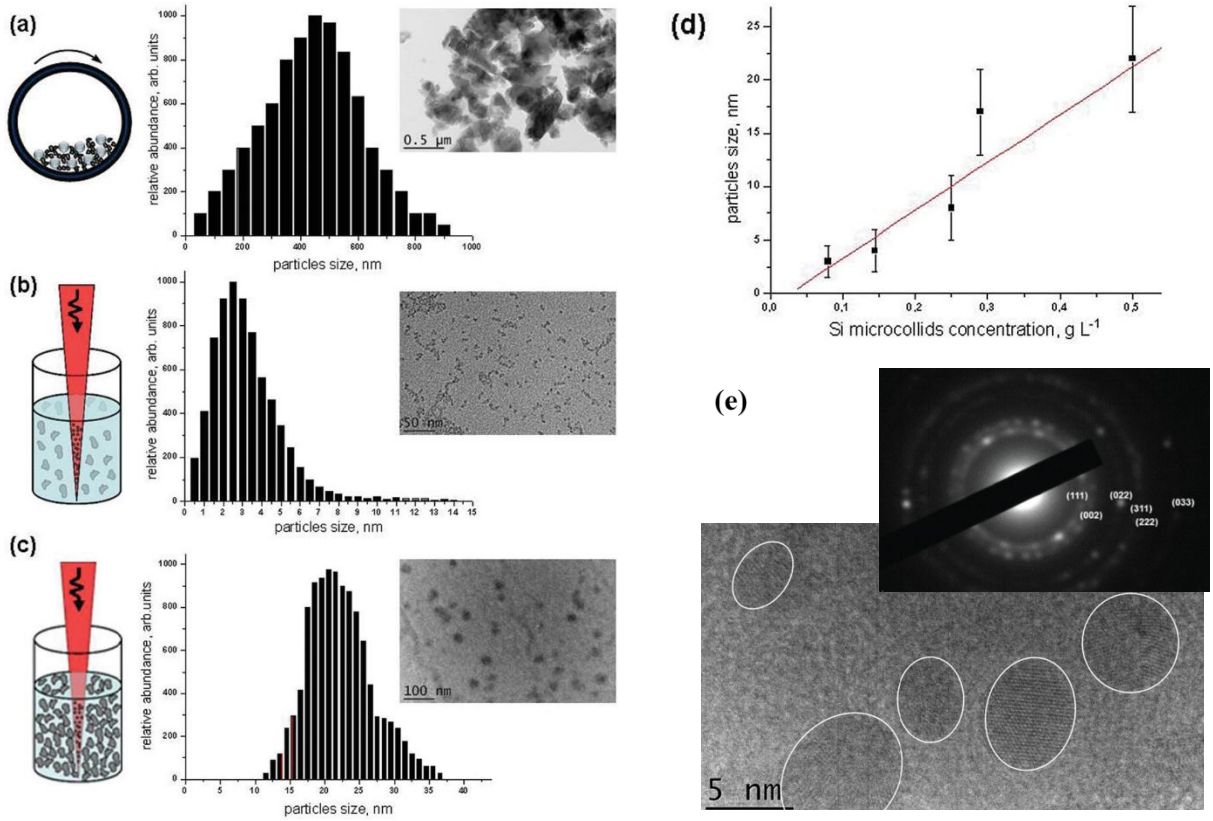

Figure 7. *(a–c) Size distributions and typical TEM images of Si particles after: mechanical grinding of c-Si wafer (a); femtosecond laser fragmentation of Si microcolloids in aqueous solutions under their low (b) and high (c) concentrations. (d) Dependence of mean size of fragmented nanoparticles on initial microcolloid concentration; (e) High-resolution TEM image and electron diffraction pattern of formed nanoparticles. Adapted from Ref. 131, 132 with permission of the Royal Society of Chemistry.*

porous Si or other counterparts prepared by wet chemistry, laser-synthesized nanoparticles prepared in deionized water do not contain any impurities on their surface, which can facilitate their direct use in biological systems.

Nanosecond laser fragmentation from pre-prepared colloids presents another interesting implementation of PLAL, which can provide quite different properties of formed nanostructures. Li[133] used an unfocused ns beam for the fragmentation of pre-prepared Si colloids and obtained a trend opposite to that observed in the fs fragmentation case, namely an increase of the final size of formed Si structures. The final product presented ideally spherical narrowly-size-dispersed microcolloids with crystalline structure. It was suggested that such structures are formed under a steady regime of laser heating, when radiation intensity is relatively low.[133]

We note that the PLAL technique provides opportunities for the formation of Si-based composite structures, as it renders possible easy mixing of different nanomaterials and their subsequent co-ablation (co-fragmentation). One promising strategy is the synthesis of nanoparticles of material A in aqueous (deionized water) or organic (acetone, ethanol) media, and then ablation of material B in the presence of nanoparticles of material A. Ablating a gold target in the presence of pre-prepared Si colloids in deionized water, we recently showed the possibility of forming Au-Si core-shell structures with controlled percentage of Si in their composition.[134, 135] A specific advantage of such nanostructures consists in the combination of plasmonic and semiconductor properties, while the Si shell surface can provide excellent biocompatibility of the core-shell.

Many studies on PLAL-based synthesis of Si nanoparticles were related to the search for conditions that yield materials with strong PL emission.[125-127, 136, 137] However, these efforts to achieve bright PL were less successful than in the case of laser ablation in gaseous environments. Here, most work reported blue (2.7-2.7 eV)[125-127] and green (2.2-2.3 eV)[137] PL bands when the ablation was performed in water or organic solutions (ethanol, *etc.*). Such PL bands are normally associated with defect-related mechanisms in SiO_x.[67, 68] Red PL associated with quantum confinement effects[70-72] was not detectable, suggesting a defect-rich structure of Si nanocrystals formed by PLAL. Svrcek[138] studied the effect of laser fragmentation on properties of water-dispersed nanocolloids of milled porous silicon, which originally exhibited strong exciton-based PL. They found that irradiation of porous silicon colloids leads to a significant quenching of the original PL and the appearance of another band in the green range, while fs laser fragmentation led to much stronger green PL signals compared to the ns case. Saitow[139-141] presented an interesting modification of PLAL by performing laser ablation in supercritical CO_2. Si nanoparticles formed under these conditions could exhibit conventional PL bands in the blue, green and red ranges, although the quantum yield of these emissions was not presented. The authors explained the reported PL properties based on the conditions of cooling of nanoclusters in supercritical fluids.

Several studies focused on the functionalization of laser-synthesized nanoparticles by organic molecules during laser-ablative processing. Such functionalizations are especially important for some potential biomedical applications. As an example, Intartaglia[142] reported 1-step conjugation of the Si nanoparticle surface by oligonucleotides by adding them to the solution during the synthesis. As another possibility, Tamarov[30] reported

conjugation of Si nanoparticles by dextrans, and a subsequent use of such conjugated complexes in cancer treatment.

Laser Pyrolysis of Silanes

Soon after the invention of the CO_2 laser, Cannon *et al.* demonstrated that CO_2 laser irradiation could be used to heat gaseous mixtures containing silane (SiH_4), initiating silane decomposition and nucleation of silicon nanoparticles.[74, 75] This is facilitated by the strong absorbance of silane at the CO_2 laser wavelength of 10.6 μm. In this laser pyrolysis process, a CO_2 laser directly heats gas phase species to a temperature (typically >1000 °C) high enough to decompose silane or other precursor gases. If the precursor gases are transparent at the laser wavelength, a photosensitizer such as SF_6 is added. The precursor stream is usually surrounded by a "sheath gas" stream, as shown in Figure 8. The sheath gas is transparent to the laser and is therefore not heated. Upon leaving the laser beam, the product particles are very rapidly cooled by mixing with unheated gas, quenching further particle growth and sintering. The small high-temperature region in which particle formation

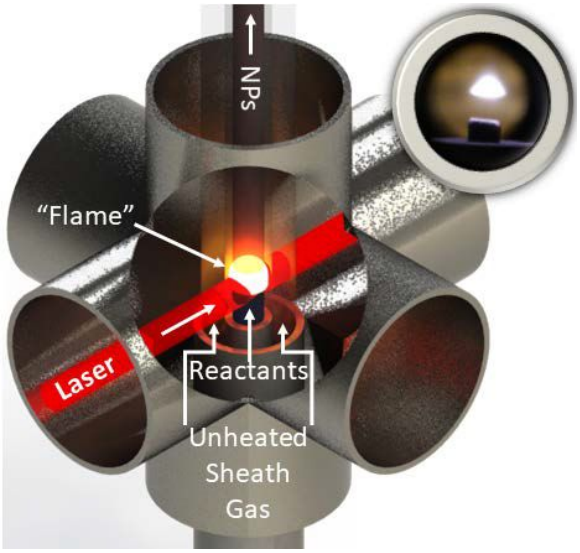

Figure 8. *Schematic illustration of laser pyrolysis reactor. The inset shows a photo of the laser "flame" that is visible in the region where the laser beam intersects the precursor gas stream.*

occurs, is often called the laser "flame". Although it is not a flame in the conventional sense, the rapid deposition of energy from the laser directly into the gas, produces visible thermal emission from the heated particles and gases that has the appearance of a flame. Laser pyrolysis provides short reaction times for precursor decomposition and particle formation (a few ms), which allows production of loosely agglomerated particles of small size at substantial production rates,[143] from hundreds of mg per hour in laboratory-scale systems to nearly kg per hour rates using high-power industrial lasers.

The laser pyrolysis method employs no solvent, gases are available in extremely high purities (*e.g.* semiconductor grade silane, of 99.9999% purity), and the reactor walls are not heated, eliminating potential sources of contamination. The particle formation atmosphere can be precisely controlled to exclude oxygen and other species that can react with silicon. In the pioneering studies of Cannon *et al.*, the silicon nanoparticles were 10 to 100 nm in size.[74, 75] However, our group showed that by tuning pressure, laser power, and the reactive environment, the mean size for silicon nanoparticles can be reduced below 5 nm.[143] This is close to the size at which silicon nanoparticles begin to exhibit efficient size-dependent photoluminescence due to quantum confinement. To produce Si nanoparticles with bright, size-dependent photoluminescence, we further etched the nanoparticles with nitric/hydrofluoric acid mixtures to produce a desired final size and photoluminescence emission color.[77, 78, 143] The photoluminescence of these nanoparticles can be stabilized *via* covalent attachment of organic ligands through hydrosilylation reactions, which also makes them dispersible in non-polar solvents.[77, 78] Attachment of ligands that make the silicon nanoparticles directly dispersible in water is possible,[144, 145] but has proven much more difficult. This combined bottom-up and top-down approach to silicon nanoparticles

synthesis is a powerful method for achieving well-controlled size and photoluminescence performance from particles produced in macroscopic quantities.

Table 1 summarizes details of various laser-based techniques to fabricate nanosilicon structures.

Table 1. Summary and comparison of different laser processing methods.

Technique	**Pulsed Laser Ablation in gaseous ambient**			**Pulsed Laser Ablation in gaseous ambient**		**Laser pyrolysis of silanes**
Configuration	PLD	LIFT	Laser spark	Long pulse ablation	Short pulse ablation	
Typical laser source	Excimer	Ti/Sapphire	CO_2	Nd/YAG	Ti/Sapphire, Yb:KGW	CO_2
Wavelength	248, 193 nm	800 nm	10.6 μm	532 nm, 1.06 μm	800 nm, 1025 nm	10.6 μm
Pulse length	20-30 ns	100-140 fs	~ 1 μs	10-20 ns	100 fs – 2 ps	~ 1 μs
Typical ambient	Buffer gas (He, Ar, H)	Air	Air	Aqueous or organic (ethanol, acetone)	Aqueous or organic (ethanol, acetone)	SiH_4 gas, H_2, or He
Final product	Nanostructured films or nanopowders, crystal size 2-4 nm, can be dispersed in liquids	20 nm – 400 nm NPs of amorphous Si, can be crystallized by laser irradiation	Nanostructured films or powders, crystal size 2-4 nm, can be dispersed in liquids	Colloidal solutions of nanoparticles, 10 nm – 500 nm, widely size-dispersed	Colloidal solutions of nanoparticles, 10 nm – 150 nm, low size-dispersed	Nanopowders, minimum crystal size 2-4 nm, tunable up to >30 nm.
Merits	High quality crystals, providing exciton PL band	Able to produce large Si NPs on a substrate	High quality crystals, providing exciton PL band	Defect-rich structure, which can enable a variety of therapies	Controllable size, defect-rich structure, which can enable a variety of therapies, fast biodegradability	High purity and crystallinity, relatively high throughput
Limitations	Wide size-dispersion after milling		Wide size-dispersion after milling	No exciton PL, wide size dispersion	No exciton PL	Post-processing required for exciton PL and dispersion in solvents

Surface Functionalization and Encapsulation in Nanocapsules

Most as-synthesized photoluminescent silicon quantum dots (Si QDs) do not form stable dispersions in water, which prevents their direct use in most biological applications. Polymer or micelle encapsulation not only makes them water dispersible, but also preserves their optical properties and protects them from oxidation and degradation.[11, 146] While we focus here on

methods applied to laser-synthesized silicon nanoparticles, consistent with the theme of this review, most of these approaches are also applicable to Si QDs produced by other means. PEG-terminated polymers form stable micelles that exhibit long circulation times *in vivo.* PEGylated phospholipids form particularly stable micelles, even at high dilution, *i.e.* they have very low critical micelle concentration (CMC). Hydrophobic materials can be transported within their hydrophobic core, while targeting agents such as antibodies, aptamers, proteins, or peptides can be attached to the micelle surface to promote localization and cellular at a disease site.

In one example, we used Pluronic® F127 and DSPE-PEG-NH_2 to co-encapsulate laser-synthesized silicon quantum dots and myristic acid.[147] Hyaluronic acid was attached to the micelle surface (Figure 9) to target CD44 (Figure 9). Such Si QDs have been used for cancer theranostics. The slow release of myristic acid from the core of the structure provides sustained delivery. In related work, we encapsulated Si QDs in Pluronic® block copolymers to make them water-dispersible for use in cancer imaging. Interaction between the poly (oxypropylene) (PPO) block of F127COOH and ethyl undecylenate attached to the Si QDs stabilized the micelles.[148] The poly

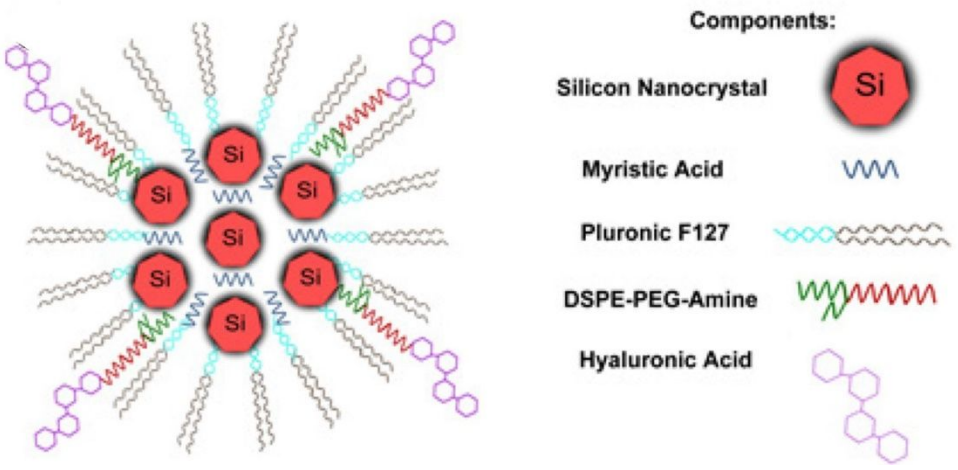

Figure 9. *Schematic of a theranostic nanoconstruct using pluronic, DSPE-PEG-Amine, and hyaluronic acid for encapsulation and targeting of Si QDs and myristic acid. Adapted from Ref. 147 with permission under a Creative Commons CC-BY license.*

(oxyethylene) (PEO) and carboxylate groups of the F127COOH formed a hydrophilic shell at the exterior surface of the micelle, making them water-dispersible.

Our group has extensively employed phospholipid micelles as Si QD carriers, with each micelle transporting many Si QDs.[11, 149] The interaction of the hydrophobic phospholipid domain of amphiphilic phospholipid-PEG molecules with the hydrophobic Si QDs produces micelles loaded with multiple Si QDs (MSi QD). This approach allows simultaneous co-encapsulation of other hydrophobic entities within the micelles (Figure 10). In one study, we functionalized Si QDs with hydrophobic moieties including styrene, octadecene, and ethyl undecylenate to make them dispersible in chloroform.[150] Transfer of these hydrophobic Si QDs into phospholipid micelles enabled their stable dispersion in water. We employed amine-functionalized phospholipid-PEGs to create luminescent probes for *in vitro* cell labeling studies.

The polymeric micelles have much lower CMC values (~10^{-6} M) compared conventional detergents like CTAB or SDS. Thus, they are much less dynamic than detergent micelles.

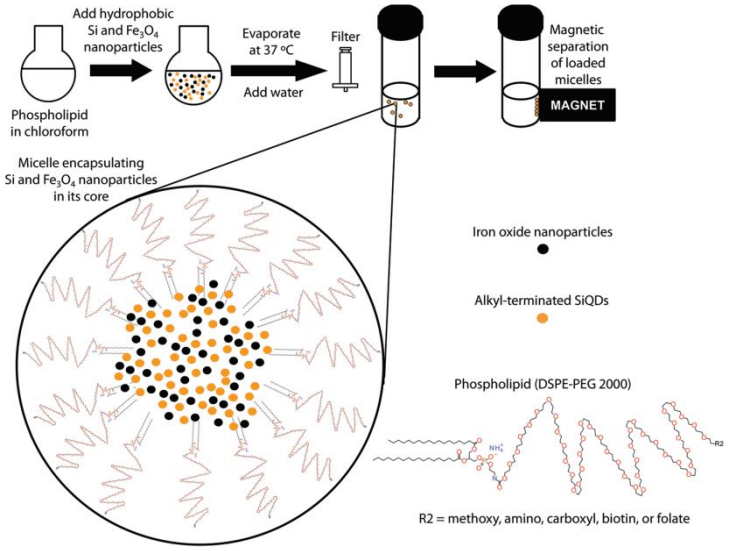

Figure 10. *Schematic illustration of co-encapsulated silicon quantum dots and magnetic iron oxide nanoparticles and their preparation. The nanoparticles are functionalized with hydrophobic ligands that interact with the alkyl chains of the phospholipid. These interactions stabilize the phospholipid-PEG micelles with multiple encapsulated nanoparticles. Adapted from Ref. 149 with permission from the American Chemical Society.*

Nonetheless, like detergent micelles, these polymeric micelles incorporate "oil-like" hydrophobic molecules or particles within their hydrophobic core. Meanwhile, the PEG layer on the exterior of the micelle is both hydrophilic and uncharged. These features extend circulation time and broaden biodistribution *in vivo*. Functionalization of a fraction of the PEG lipids with specific groups facilitates the attachment of targeting moieties to promote delivery to particular tissues or cell types.

Applications of Laser-Processed Nanosilicon

Applications in Energy

Silicon nanoparticles, including those prepared by laser-based methods, can be used in a wide range of energy-related applications that take advantage of their optical, electronic, and chemical properties. Among other possibilities, they can serve as absorbers in photodetectors or solar cells,[151-155] serve as emitters in LEDs,[156-159] be used as photoluminescent components in solar concentrators,[160] react with lithium ions in high-performance anodes for lithium ion batteries,[161, 162] and be used in hydrogen generation *via* reaction with water.[23] This section briefly describes specific selected examples of these applications in which laser-synthesized silicon nanoparticles have been employed. For some of these applications, particularly where large quantities of nanoparticles are needed and costs must be low, other nanostructuring methods may be more appropriate than laser processing. Nonetheless, nanoparticles from laser processing can be quite valuable in demonstrating these applications and developing devices.

Photovoltaics and Photodetectors. Silicon, in the form of single-crystalline or polycrystalline wafers, is the dominant material used for photovoltaics and photodetectors for visible light, from the CMOS cameras in cell phones to large-scale solar power installations. Silicon, as an indirect bandgap material, is inherently a weak absorber of visible light, so these bulk silicon devices rely on thick silicon layers for light absorption. One manner in which silicon nanoparticles have been used in conventional silicon photovoltaics is in preparation of silicon inks for fabrication of selective emitter structures by screen printing on top of conventional silicon solar cells. The Dupont Innovalight Cougar™ process provides one example of this approach.[163] However, such applications do not rely on any special properties of the silicon nanoparticles, other than the ability to formulate them into a screen-printable ink. Theoretical studies have described the potential of silicon nanoparticles in third-generation photovoltaics that achieve carrier multiplication.[164] However, many challenges related to weak absorbance of silicon and poor charge transport within silicon nanoparticle films remain to be overcome before such devices can be realized.

Silicon absorbs strongly at UV wavelengths, below about 365 nm (3.4 eV), where a direct band-to-band transition can occur. Thus, a thin film of luminescent silicon nanoparticles can enhance the efficiency of conventional silicon solar cells by serving as down converters – absorbing UV wavelengths that are poorly harvested by the underlying solar cell, and re-emitting at wavelengths well-matched to the underlying solar cell. Such approaches have been demonstrated with Si QDs produced by electrochemical etching,[165] nanosecond pulsed laser ablation,[166] and low-pressure plasma[167] methods, among others. Si QDs from these different methods, and others, have produced similar levels of enhancement of overall

power conversion efficiency, up to a few percent, but direct performance comparisons are not possible, because each study used different underlying solar cells with different efficiencies and wavelength responses.

One can also exploit the UV absorbance of silicon to create a UV-sensitive photodetector by using silicon nanoparticles as the only absorber in the device. We demonstrated this using laser pyrolysis of silane followed by HF etching to produce H-terminated silicon nanoparticles. We then grafted diallyl disulfide to the surface of the nanoaprticles.[151] This laser synthesis and surface functionalization allows production of a high-quality colloidal silicon nanocrystal ink with short covalently bound surface ligands that allow reasonable charge transport within a solid film of the nanocrystals. In addition to the spin-cast film of functionalized silicon nanocrystals, the finished device included a poly(3,4-ethylenedioxy-thiophene):poly(styrene sulfonate) (PEDOT: PSS) electron blocking layer and top- and bottom-contacts. Photogenerated charge separation in the device was driven by the

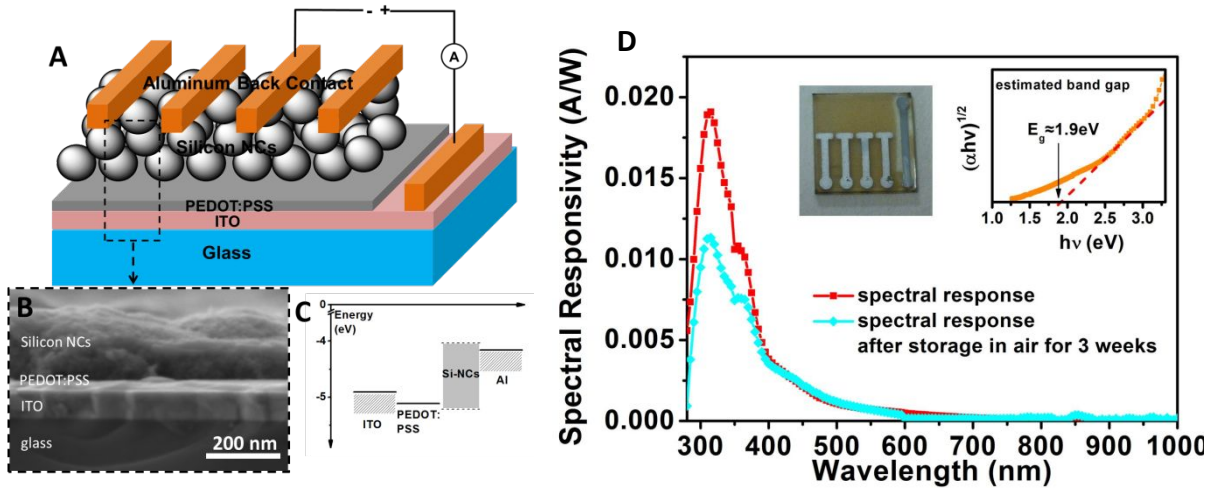

Figure 11. *Structure and characterization of a silicon nanocrystal-based UV photodetector, A) Overall device structure, B) Actual device imaged with SEM, C) device energy band diagram, and D) Spectral responsivity before (red curve) and after (blue curve) 3 weeks of storage in air. Indirect bandgap estimation by the Tauc method and a photograph of representative SiNC devices are shown as insets. Adapted from Ref. 151 with permission from John Wiley and Sons.*

Schottky-junction formed at the interface between the Al back electrode and the silicon nanocrystal layer. Figure 11 illustrates the device structure and its performance. The peak photoresponse of 0.02 A W^{-1} at UV wavelengths, from the unpackaged diode, is approaching that of III-V and SiC-based UV photodetectors that are commercially available. This provides a route to large-area solution-processed UV photodetectors and demonstrates the potential of inks formulated from laser-processed silicon nanocrystals for broader applications in solution-processed optoelectronics. Alkis *et al.*[154] took a different approach in which they coupled silicon nanoparticles produced by laser ablation to plasmonic silver nanoparticles to achieve enhanced visible response in a silicon nanoparticle-based photodetector. Yu *et al.*[168] combined nonthermal-plasma synthesized silicon quantum dots with graphene to fabricate a photodetector with very impressive performance. This same approach could be taken with laser-synthesized Si QDs. Unfortunately, direct comparisons between photodetector performance achieved with Si QDs from laser pyrolysis, laser ablation, and low-pressure plasma synthesis is hindered by the fact that each study used a different device architecture.

Laser-synthesized silicon nanoparticles have also been incorporated into organic photovoltaic devices, where they have provided improved overall efficiency and higher open circuit voltage. In one study, we demonstrated a hybrid organic-inorganic photovoltaic device that combined poly(3-hexylthiophene) (P3HT)/[6,6]-phenyl-C61-butyric acid methyl ester (PCBM) with silicon nanocrystals from laser pyrolysis. The Si NCs were etched with HF and then mixed with P3HT/PCBM without any additional surface modification.[153] Adding the Si-NCs to the bulk heterojunction device produced an extended optical excitation response and increased the short-circuit current by 26%.

In a separate study, we incorporated silicon nanoparticles into hybrid organic-inorganic photovoltaics without including P3HT as an absorber.[152] In this case, PCBM and PEDOT:PSS served as electron and hole transport layers, respectively. The silicon nanoparticles were sandwiched between the PCBM and PEDOT:PSS. This study focused on relating the solar cell performance to the size of the silicon nanoparticles. We showed that both the size of the Si-NCs and their crystallinity (amorphous fraction) affected the open circuit voltage (V_{OC}) of the device. Both of these properties can be tuned by varying the operating conditions in the laser pyrolysis process. Band-gap widening in smaller or less crystalline (higher amorphous fraction) silicon nanoparticles increases the V_{OC} when PCBM is used as the acceptor in the device. The observed V_{OC} reached 0.634 V in a cell made with 5.7 nm Si-NCs. However the overall efficiency remained low, because of the relatively weak absorbance of the thin film of silicon nanocrystals and the poor charge transport through the Si-NC film. Another study, using commercially-available silicon nanoparticles (of uncertain production method) found a detrimental effect of their incorporation into a P3HT/PCBM organic photovoltaic device.[169]

Meinardi *et al.*[160] demonstrated the use of Si QDs in luminescent solar concentrator systems, in which the Si QDs embedded in a window film absorb UV light and emit visible light that is guided to the window edges, where it is used by conventional photovoltaic devices. This work employed Si QDs from nonthermal plasma synthesis, but such devices could equally-well employ laser-synthesized Si QDs. This is a particularly promising application of Si QDs because it relies on absorbance of UV wavelengths, where silicon is a strong absorber, and requires minimal re-absorption of emitted light by the absorber. Based on the similar performance of Si QDs of different origin as down converters in films deposited atop silicon solar cells, one would also expect similar performance here.

Silicon Nanoparticle-based Lithium Ion Battery Anodes. Silicon has exceptional potential as an anode material for lithium ion batteries. Its theoretical gravimetric capacity for lithium ion storage is more than ten times that of graphite, which is used in the anodes of most current lithium ion batteries. However, silicon anodes are subject to poor cycling performance due to mechanical failure, pulverization, and formation of an unstable solid-electrolyte interphase (SEI) layer. Silicon nanostructures can accommodate significantly greater stress and strain than bulk silicon, and also have higher electrolyte-accessible surface area and shorter electronic and ionic transport distances, improving rate capabilities. Unfortunately, this can also increase the area for SEI formation. Thus, a huge amount of research effort has been devoted to developing silicon nanostructures for use in lithium-ion batteries and to stabilization of the SEI on silicon anodes. Much of this work

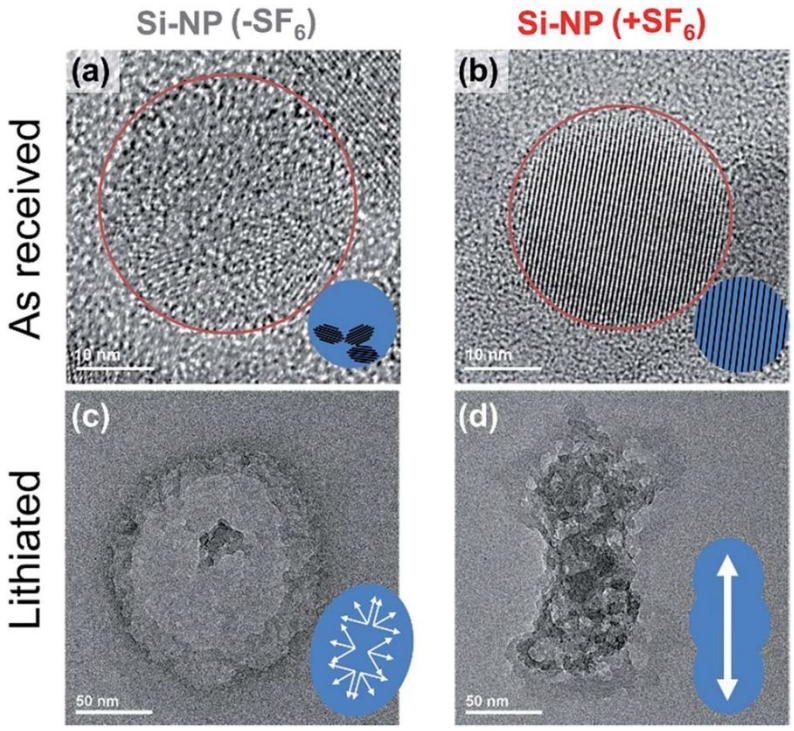

Figure 12. *HR-TEM images of an amorphous Si nanoparticle (-SF6; panels a and c) and a single crystalline Si nanoparticle (+SF6; b and d) before (a and b) and after (c and d) lithiation. From Ref. 161. Used with permission from the Royal Society of Chemistry.*

was recently reviewed by Ryu *et al.*[170] Relatively few studies have considered the use of laser-synthesized silicon for lithium ion batteries, because the large-scale use of silicon in this application will require production at extremely low cost (<$100/kg). Nonetheless, the ability to control size, purity, and crystallinity using laser-based processing could prove advantageous in understanding the performance of silicon nanostructure-based anodes.

In one study that specifically focused on laser-based synthesis of silicon nanoparticles for use in lithium ion battery anodes, Kim *et al.*[161] optimized their reactor conditions to achieve 97% conversion of silane to silicon by laser pyrolysis, producing ~20 nm, single-crystalline silicon nanoparticles that performed well as a lithium ion battery anode material. In addition to achieving high utilization of silane (which is essential for keeping cost down), this study demonstrated the ability to control the crystallinity of the product Si nanoparticles by varying the amount of sulfur hexafluoride (SF_6) used as a photosensitizer to absorb the laser energy. Although silane directly absorbs the CO_2 laser energy, SF_6 is a much stronger absorber, and can therefore be used to produce a much higher temperature in the laser pyrolysis process. As shown in the top two panels of Figure 12, this allowed production of amorphous or poorly-crystalline Si nanoparticles (panel a) without SF_6 or highly crystalline Si nanoparticles (panel b) using an appropriate amount of SF_6. Although the Si nanoparticles become amorphous upon lithiation (panels c and d), the initially crystalline particles expand anisotropically (panel d), which allowed them to better accommodate the stress and strain associated with volume change during cycling. As a result, the highly crystalline Si nanoparticles showed much better capacity retention than the amorphous or poorly-crystalline particles, especially at high charge-discharge rates. This provides an example of how the control of size and crystallinity provided by laser-based processing of silicon nanoparticles can play an important role in the application of silicon nanoparticles in lithium ion batteries.

Several studies have employed pulsed laser deposition to produce nanostructured silicon films for use as lithium ion battery anodes.[171] Radhakrishnan *et al.* used PLD to deposit nanostructured silicon on multilayer graphene that had been grown by chemical vapor deposition on a nickel foam substrate.[172] The resulting anodes exhibited impressive capacity and better stability than pure silicon anodes, but they were only tested for a few cycles. Biserni *et al.* first deposited nanostructured silicon by PLD, then overcoated it with carbon by CVD.[173] Garino *et al.* employed alternating PLD of silicon and carbon to make nanostructured multilayered Si/C films for use as anodes in microbatteries.[174] They showed that controlling the porosity of the multilayer structure was a key to achieving both good performance and relatively good stability of the anode.

Hydrogen Generation by Reaction of Silicon Nanoparticles with Water. Another energy-related application of silicon nanoparticles is on-demand generation of hydrogen by reacting them with water.[21-23] In such a system, the silicon nanoparticles essentially serve as a source of stored energy, while the water serves as a carrier of hydrogen. Aluminum and other water-reactive metals can be used in a similar manner and aluminum, in particular, has been much more heavily studied for this application than silicon.[175] Silicon has the advantage of providing four electrons per silicon atom allowing each silicon atom to react with two water molecules to produce two H_2 molecules and one formula unit of SiO_2. As a result it has a higher theoretical gravimetric capacity for hydrogen generation than aluminum, and in combination with a hydrogen fuel cell can provide an exceptionally high energy density source of electricity, substantially exceeding that of the best batteries. More recently, boron has been used in a similar manner.[176] It has much higher theoretical gravimetric capacity for hydrogen generation than either silicon or aluminum, but suffers from relatively high cost and low reactivity with water.

In our study of hydrogen generation by reaction of silicon nanoparticles with water, we demonstrated that nanosize silicon (~10 nm diameter) prepared by laser pyrolysis of silane reacts with water, *via* base-catalyzed silicon etching, to generate hydrogen 10,000 times faster than bulk silicon.[23] The H_2 production rate achieved using 10 nm Si was 150 times that observed for 100 nm particles. This rate increase is much too large to be explained by the increased surface to volume ratio of the smaller particles. The dramatic rate increase reflects change in the dynamics of the etching process at the nanoscale. Larger silicon particles are etched anisotropically, while etching of the 10 nm silicon is effectively isotropic. Figure 13 summarizes these results, comparing silicon of different sizes and providing comparisons to prior studies. Figure 13(c) demonstrates that hydrogen produced by reaction of silicon nanoparticles with water can be used directly in a fuel cell. Here, the first key advantage of the laser pyrolysis synthesis of silicon is the ability to produce sufficiently small (~10 nm) particles to allow their complete and rapid base-catalyzed reaction with water. Because this base-catalyzed reaction is anisotropic, larger particles rapidly become faceted, leaving only unreactive surface. They therefore do not fully react. Moreover, because the nanoparticles are synthesized in a hydrogen-rich environment, they are produced with hydrogen bound to their surfaces. This hydrogen is released during the reaction with water, such that the actual amount of hydrogen produced even exceeds the theoretically expected yield (two H_2 molecules per Si atom). Even if the particles were not hydrogen-terminated, they could still react in the same manner. However, surface oxidation can significantly reduce the gravimetric hydrogen generation capacity, both by reducing the amount of silicon available for reaction and by adding mass (of oxygen). Here, the hydrogen termination of silicon particles produced by laser pyrolysis in hydrogen, provides an advantage over other synthesis methods that do not produce a hydrogen-terminated surface.

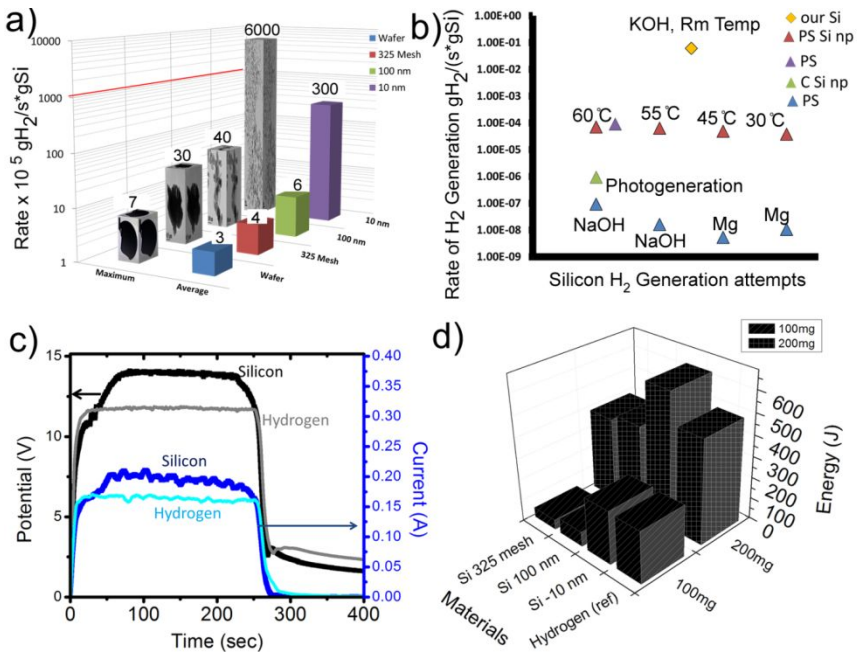

Figure 13. *Rates of hydrogen generation and silicon and fuel cell performance using hydrogen produced by reaction of water and silicon. (a) Rates measured using different forms of silicon, with maximum and average rates in the left and right columns, respectively. (b) Rates reported in the prior literature and in Ref. 23 (see original paper for details) c.) Comparison of current and voltage outputs from a fuel cell using H_2 generated on demand from water and silicon nanoparticles compared to pure hydrogen in the amount expected by reaction of the amount of silicon used. d) Energy output from the fuel cell using different hydrogen sources. From Ref. 23, used with permission from the American Chemical Society.*

While our work with silicon produced by laser pyrolysis demonstrated how small particle size and hydrogen termination were advantageous for hydrogen generation by reaction of silicon with water, the practical prospects of using laser-processed silicon for this application are limited. Thus, others have focused on use of additives and processing strategies with lower-cost, larger-size silicon. Kobayashi *et al.*[177] and Xu *et al.*[178] used ball milling (or bead milling) to reduce the silicon particle size to a range where hydrogen generation was effective. Brack *et al.*[179] explored the formation of nanocomposite pellets of silicon with additives such as sodium hydroxide to increase the rate of hydrogen generation. Approaches like these can employ very low-cost starting materials, such as waste from the photovoltaics industry or commodity ferrosilicon. Nonetheless,

the practicality of any of these approaches remains to be fully demonstrated, and significant questions remain.[180]

Applications in Nanobiotechnology:

Biological Assessment of Nanosilicon Prepared by Laser Processing. Si nanostructures occupy a particular niche related to biomedical applications. Excellent biocompatibility of Si nanoparticles and its oxide form, silica (SiO_2), are well known and described in the literature.[32-34] However, in contrast to silica, Si nanoparticles have an additional biodegradability option, which provides a decisive advantage for biomedical applications. Indeed, in the aqueous biological environment, Si nanostructures can decompose into orthosilicic acid, $Si(OH)_4$, which is then excreted in the urine. The biodegradability effect was studied for ultrasonically milled and water-dispersed porous silicon-based nanostructures prepared by electrochemical etching in HF/ethanol solutions.[5] Those studies found that Si nanostructures can indeed biodegrade and completely dissolve in biological matrices and then be excreted from the body. However, due to the wide range of sizes and shapes of porous silicon-based nanostructures, their biodegradation was slow and could take more than 4-6 weeks.[5] We recently studied dissolution of Si nanoparticles prepared by laser fragmentation in deionized water.[6, 132] In contrast to porous Si-based structures, such nanoparticles were spherical and with low polydispersity, which was expected to contribute to better transport *in vivo*. We found that the dissolution rate of Si nanoparticles was dependent on the concentration of oxygen defects in the crystalline Si core, which could be controlled by the content of dissolved oxygen in the aqueous ambient during the synthesis. Dense low-defect Si nanoparticles synthesized under oxygen-free condition (when dissolved oxygen removed Ar gas bubbling) completely dissolved after 2-3 weeks (Figure

14a), as recorded by TEM and Raman spectroscopy. In contrast, oxygen defect-rich nanoparticles prepared in oxygen-rich conditions (no bubbling) exhibited a much faster dissolution kinetics and were mostly dissolved after 4-7 days (Figure 14a). This study illustrates an important reason for the strong potential of Si nanoparticles for applications in biological systems.

In vitro tests We recently studied the interaction of Si nanoparticles with biological matrices *in vitro* and *in vivo*.[6, 30, 132] We did not observe any notable cytotoxicity toward human cells (HMEC) up to concentrations of 100 μg mL^{-1} (cell survival rate exceeded

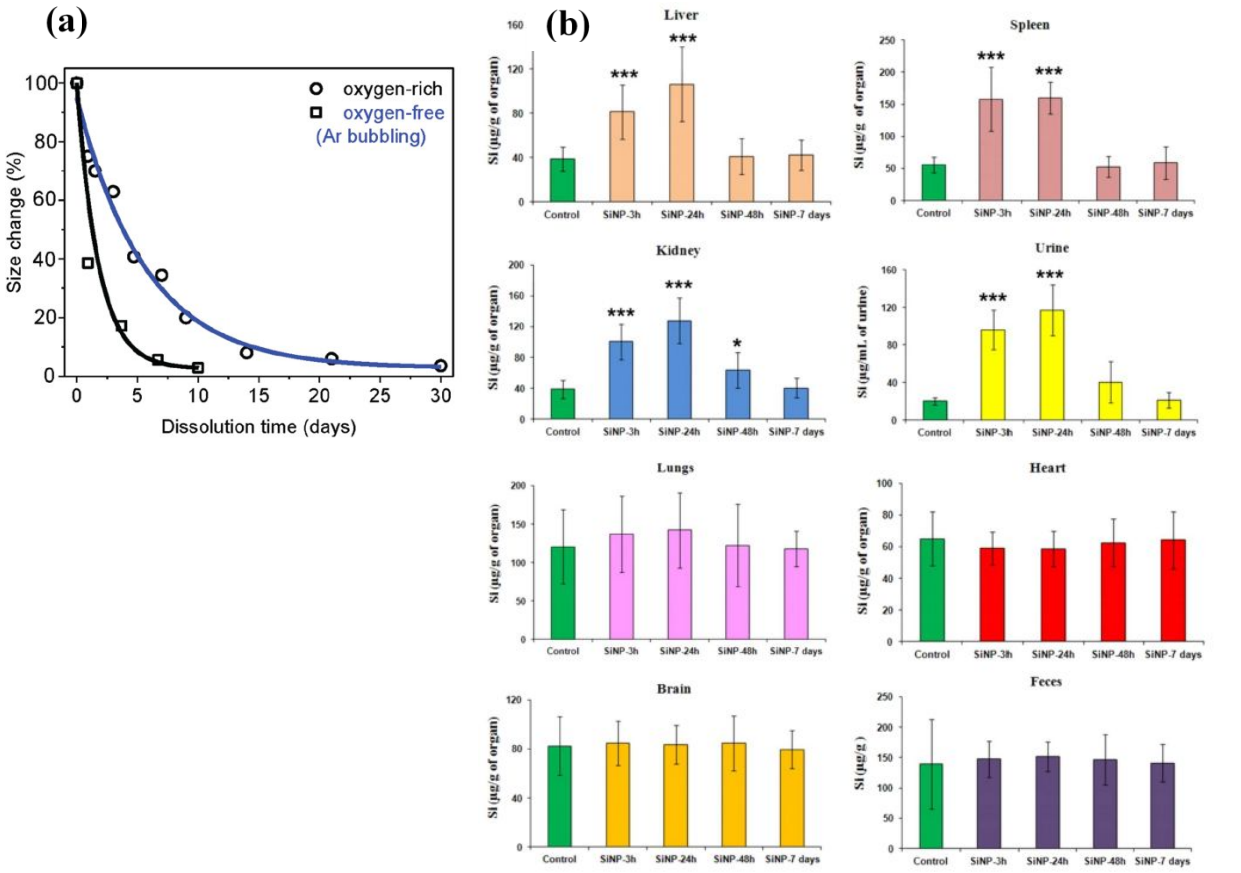

Figure 14. *(a) Time evolution of the size of Si-nanoparticles prepared by femtosecond laser fragmentation in oxygen-rich (black) and oxygen-free (blue, Ar bubbling) water ambient, under nanoparticles aging in deionized water. Adapted from Ref. 132 with permission from the Royal Society of Chemistry; (b) Content of Si in mice organs and biological fluids after systemic administration with Si nanoparticle-based aqueous solutions (20 mg/kg) 3 h, 24 h, 48 h and 7 days after the injection related to mice control group. Adapted from Ref. 6 with permission under a Creative Commons CC-BY license.*

80%).[132] We also found from electron microscopy that Si nanoparticles were taken up by cells *via* an endocytosis mechanism.

In vivo tests. To study the effect of Si nanoparticles on biological systems, we recently studied the biodistribution, in a mouse model, of laser-synthesized nanoparticles.[6] Here, the worst scenario was considered, in which the nanoparticles were non-functionalized by PEG and should have been immediately sequestered by the reticuloendothelial system. Four groups of mice were systemically administered in the jugular vein with a single dose of 20 mg/kg of Si-nanoparticles in physiological solution and then examined at different moments after the administration of nanoparticles. All animals remained healthy and exhibited normal activity after nanoparticle administration. The body weight of mice from Si nanoparticle-treated and control groups remained similar. To study biodistribution of Si nanoparticles, we quantified Si concentration in different organs, including liver, spleen, lungs, heart, *etc.*[6] Here, during first hours we observed ab increase of silicon content mostly in the liver and spleen, evidencing a rapid sequestration of Si nanoparticles by the reticuloendothelial system (Figure 14b). We then recorded the increase of Si concentration in the kidneys and urine (24 h after administration), and its further progressive decrease. After 7 days, we observed the return of Si content down to normal values in all matrices. We observed only minor inflammation in hepatocytes during histopathological examination of liver tissues, which disappeared 48 h after the injection. Such a result contrasts to previous data on intravenous injection of silica (SiO_2) nanoparticles, presenting an oxidized non-dissolvable form of silicon, whose accumulation in the liver led to major damages.[181] Similar clearance of Si nanoparticles within 48 hours was detected from histopathological examination of spleen and kidney. We determined that the nanoparticles

then biodegraded and silicon was eliminated in the urine without any side effects. Our biochemical studies confirmed that the injection of Si nanoparticles did not induce any liver or kidney toxicity, as was confirmed by ALAT, ASAT and serum creatinine levels, which were still similar to that of the control group. We additionally did not detect any significant change of oxidative stress parameters including catalase, SOD, GPx activities, Vit A, E72, as well as no significant variation in the blood content.[6, 30]

We have also done a thorough study of the *in vivo* cytotoxicity of silicon quantum dots (Si QDs) from silane laser pyrolysis that were surface functionalized with ethyl undecylenate (undecylenic acid), and encapsulated in pluronic F127,[182] similar to the approach illustrated in Figure 9. Both ethyl undecylenate and pluronic F127 are non-toxic FDA-approved substances, so any toxicity in this case could be attributed to the Si QDs. For this study, we took great care to optimize the surface passivation to achieve high photoluminescence quantum yield (36%) and long-term chemical and colloidal stability. We then tested the toxicity of these materials in both mice and monkeys (rhesus macaques). We used a very aggressive dose of 200 mg/kg body mass, based on the expectation of low toxicity from these formulations. Even at this high dose, the behavior, body mass, and blood chemistry of both the mice and monkeys remained normal. However, in contrast with other *in vivo* studies of silicon, we did not observe biodegradation of this silicon formulation. Three months after intravenous injection of Si QDs, the livers and spleens of mice still showed elevated silicon content. At this same time point, histopathology indicated detectable adverse effects in the livers of mice, but not in monkeys. One key lesson from this study is that thorough passivation of silicon nanoparticles with covalently-linked organic molecules, to achieve high quantum yield and chemical stability of the Si QDs, can also prevent degradation of the Si QDs. The silicon-carbon bonds at the Si QD surface do not undergo hydrolysis, and the

organic surface layer protects the Si QDs from degradation. The other key outcome of this study is that observations made in mice, which are the most common animal model used for assessing toxicity of nanomaterials, may not be applicable to primates.

In general, our tests evidenced the complete safety of laser-synthesized nanoformulations, and show that silicon itself is effectively degraded and eliminated. However, formulations in which the silicon is carefully protected to preserve its properties, may not biodegrade, or may undergo much delayed degradation. Thus, surface chemistry and encapsulation strategies should be carefully considered to achieve a balance between preserving desirable properties and ensuring degradation and clearance *in vivo*. The appropriateness of laser-synthesized silicon vs. silicon from other methods, such as the porous silicon particles employed by Sailor and coworkers,[5, 12] depends upon the specific application, as each material will exhibit different biodistribution, degradation kinetics, capacity to serve as a carrier for other agents, and spectral and temporal response to illumination.

Optical Biosensing, Bioimaging and Multimodal Imaging. As shown in previous studies using porous silicon, PL emission from nanosilicon crystals can be efficiently quenched by exposure to various organic and inorganic molecules. Such quenching can be explained by both energy- and electron-transfer mechanisms.[183] The use of this quenching effect for sensing of various chemical substances and biological molecules has been proposed and demonstrated. Based on the same PL quenching effect, laser-synthesized nanosilicon crystals prepared by PLD were also explored as matrices for biosensing to characterize inorganic nanoparticles (WO_3, W_2O_5)[184] and sense organic aromatic nitro compounds.[185] In a separate study, porous nanosilicon layers, deposited on a gold film by PLD in residual helium gas, were explored as matrices for bioimmobilizations in Surface Plasmon Resonance biosensing[186] based on a Si prism platform.[187] The employment of such a

matrix makes possible the maximization of probed material by a much-enhanced surface area for immobilizations.

The size-dependent PL emission wavelength, narrow width of the emission band, and broad excitation spectrum of quantum dots (QDs) have made them valuable for optical bioimaging. However, for cadmium-based QDs, which are the most widely investigated, toxicity associated with cadmium is a major barrier to broad use. Si QDs are less toxic. However, stably dispersing Si QDs in biological media has been a major challenge. Availability of water-dispersible Si QDs represents a significant advance in both *in vitro* and *in vivo* QD-based optical imaging. Water dispersible Si QDs can be prepared by directly functionalizing the Si QD surface with a carboxylic acid group or an amine group. However, water dispersed Si QDs generally exhibit poor colloidal stability weakened photoluminescence in aqueous solutions. Tilley *et al.* attached allylamine to Si QDs to make them water-dispersible.[38, 188] Ruckenstein and coworkers grafted poly-acrylic acid onto Si QDs from with red photoluminescence, initially produced by silane laser pyrolysis, and demonstrated fixed cell labeling using these hydrophilic Si QDs.[189] Our group functionalized Si QDs with acrylic acid in the presence of HF, to prevent oxidation.[144] We showed *in vitro* uptake of Si QDs encapsulated in micelles of amine-functionalized phospholipid-PEGs into pancreatic cancer cells by confocal imaging.[11] Our Si QD-based probes are not enzymatically degraded or rapidly captured by the reticuloendothelial system (RES), remain stable in the acidic tumor microenvironment, and show stable bright photoluminescence *in vivo*. This combination of properties makes them attractive for clinical applications including image guided drug delivery, mapping of sentinel lymph nodes (SLN), and visualization of tumor margins (Figure 15).

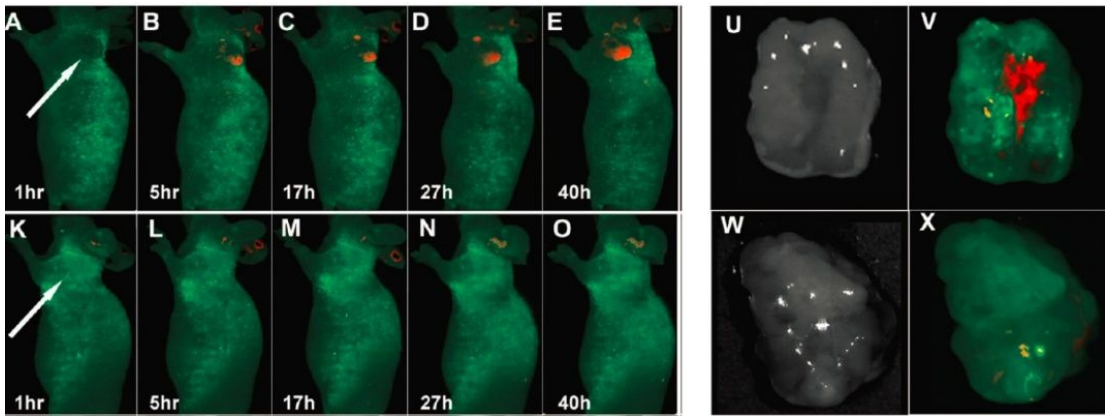

Figure 15. *In vivo imaging of mice with xenograft Panc-1 tumors (white arrows) at the indicated times after injection with ~5mg of (A-E) targeted MSi QD-RGD or (K-O) untargeted MSi QD. Autofluorescence and Si QD emission are shown as green and red, respectively. Ex vivo photographs (U, W) and luminescence images (V, X) of tumors from mice treated with (U, V) MSi QD-cRGD or (W, X) MSi QD, excised 40 h after injection. Adapted from Ref. 150 with permission from the American Che mical Society.*

We demonstrated *in vivo* imaging using Si QDs.[150] PEGylated micelle encapsulation and bioconjugation yielded a formulation with stable luminescence and long (>40 h) circulation and tumor accumulation time. Thus Si QDs can be suitable for use in sophisticated *in vivo* models. The Si nanoparticles also allow for incorporation of other modalities of imaging as multimodal nanoparticle platforms are desirable for application in cancer nanotechnology. One such example is a single nanoplatform that exhibits both photoluminescence and localized surface plasmon resonance (LSPR) based scattering and absorption Here the challenge has been to overcome attenuation of optical emission caused by nonradiative decay due to plasmonic interactions. To combine gold with silicon quantum dots, we created Si QD core/Au shell constructs in which the Au and Si were separated to preserve each of their optical properties.[148] We employed surface FDA-approved ethyl undecylenate for surface passivation of the Si QDs. Multiple silicon quantum dots were encapsulated within each pluronic F127-COOH polymer micelle. The resulting water dispersible formulation has two key benefits compared to Si/Au core–shell nanostructures based on single Si QDs: (i) fluorescence from many Si QDs within each F127 micelle produces much

brighter emission from each nanocapsule; and (ii) rather than being attenuated (quenched) by interactions with gold, the Si QD luminescence may even be enhanced *via* plasmonic amplification of local electric fields by the gold shell. Our approach for producing these Si–Au hybrid core–shell nanostructures is illustrated in Figure 16.

We modified surface of Si QD-COOH with poly-L-histidine (PLH), which efficiently immobilizes gold ions.[190-192] The Au^{3+} was then reduced by NH_2OH to form a gold shell (yellow circle) which exhibits plasmonically-enhanced light scattering that is useful for dark field imaging. Meanwhile, the Si QDs remain photoluminescent (Figure 17). We demonstrated multimodal imaging of pancreatic cancer cells and showed that the Si QD photoluminescence coincided with light scattering from the gold shells.

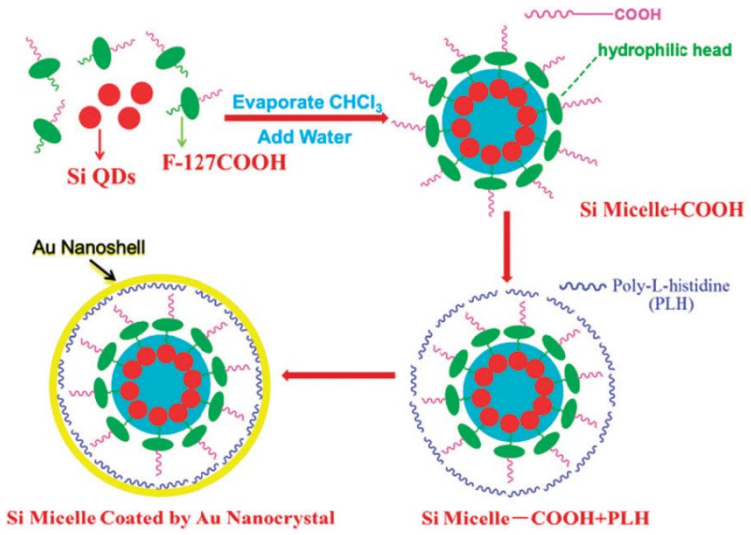

Figure 16. *Si/Au hybrid nanostructures (golden-Si QD). Mixing functionalized Si QDs (red) with F127-COOH (green F127 and purple COOH) led to micelle encapsulation of the Si QDs. PLH (blue squiggles) was electrostatically attached to the micelle surface then used to immobilize Au^{3+}. Gold reduction using NH_2OH produced a gold shell (yellow circle). The components are not drawn to scale. From Ref. 148, used with permission from Oxford University Press.*

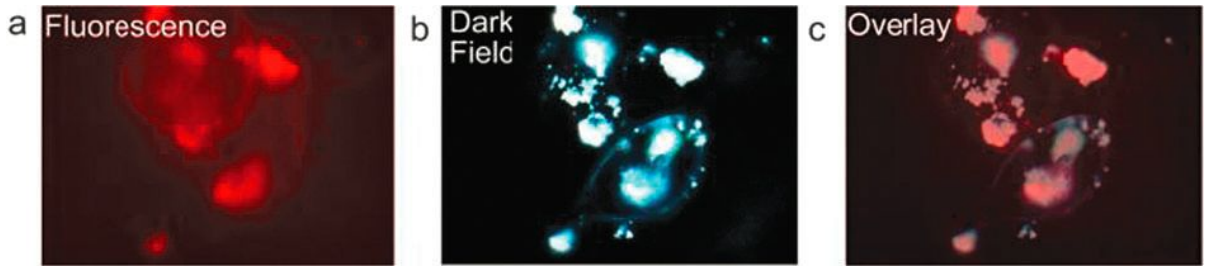

Figure 17. *Fluorescence and dark-field imaging of pancreatic cancer cells treated with golden Si QDs, (a) fluorescence micrograph obtained with 400 nm excitation and 600 nm emission filter, (b) dark-field microscopy micrograph, (c) dark field micrograph overlay on the fluorescence micrograph. From Ref. 148, used with permission from Oxford University Press.*

Iron-oxide nanoparticles, manganese, and gadolinium have been combined with Si QDs to produce nanoplatforms for both optical and magnetic resonance imaging.[149] The luminescence of Si QDs was attenuated in the presence of the iron oxide particles. Doping of silicon quantum dots with manganese for MR imaging has also been demonstrated, but manganese doping also lowers the photoluminescence quantum yield of the Si QDs.[193] Nonetheless, in both cases (iron oxide and manganese) the emission remained bright enough to be useful.

Chelated Gd^{3+}, with seven unpaired electrons that respond strongly to an applied magnetic field, is a popular MRI contrast agent.[194] This local magnetic field produced by Gd^{3+} reduces the relaxation time of nearby water protons,[195] providing contrast between tissues that have taken up Gd^{3+} and those that have not. MRI validated with NIR optical imaging can be effective for breast cancer imaging. Gd^{3+} in close proximity to quantum dots in quantum dot–Gd^{3+} complexes has been shown to increase luminescence quantum yield.[196] The low tumbling rate of QDs, combined with their ability to carry many Gd^{3+} ions, enhances the sensitivity of molecular MRI. Many challenges must be surmounted in order to prepare and apply multimodal nanoconstructs containing both quantum dots and Gd^{3+} moieties. Aptekar *et al.*[197] reported the use of silicon nanoparticles as hyperpolarized magnetic resonance imaging agents; however, they were larger in size and thus were not quantum dots. Tu *et al.* studied Mn-doped Si QDs for MRI and two photon

optical imaging of macrophages.[198] However, Si QDs with emission at longer wavelength are more desirable to reduce light absorption and autofluorescence from tissues.

We developed luminescent, MRI nanoconstructs comprising Si QDs encapsulated in DSPE-PEG (1,2-distearoyl-sn-glycero-3-phosphoethanolamine-N-[amino(polyethylene glycol)-2000] (ammonium salt)) micelles with DOTA-chelated Gd^{3+} covalently attached to their surface.[199] DSPE-PEG micelles provide long circulation times by avoiding uptake by the reticuloendothelial system (RES). The hydrodynamic diameter of these nanoconstructs ranged from 25 to 60 nm. The magnetic resonance relaxivity in the presence of these nanoconstructs was 2.4 mM^{-1} s^{-1} (where the concentration is that of Gd^{3+} ions). This value corresponds to around 6000 mM^{-1} s^{-1} based on the concentration of overall nanoconstructs. We measured both optical and magnetic properties of these structures, then used them for imaging in macrophage cells and live mice. We also demonstrated magnetic field enhancement of cellular uptake *in vitro*.

We have recently demonstrated use of Si nanoparticles formed by laser-plasma ablative synthesis in gaseous helium as markers for bioimaging.[13] Si nanocrystals exhibiting strong exciton-based PL around 1.5-1.75 eV (750-850 nm) were originally formed by PLD and then milled by ultrasound and dispersed in aqueous solutions. The nanoparticles were incubated *in vitro* with a CF2Th cancer cells. Figure 18 shows confocal fluorescent microscopy images of cancer cells with incubated nanoparticles, in which the cell nuclei and cytoplasm are labelled by blue and green, respectively. Figure 18a shows cells in different proliferation states, including mitotic cells in the metaphase, which provides evidence of normal cell proliferation in the medium containing Si nanoparticles. As follows from Figure 18b,c, laser-synthesized Si nanoparticles emit different PL bands, which is in good agreement with their PL spectra in water (Figure 18a), while the control group does not show any signal (Figure 18d). It is also important that Si nanoparticles can

penetrate into the cytoplasm, but do not enter into the cell nuclei, which excludes potential gene toxicity problems.

We finally assessed Au-Si core-shells prepared by methods of femtosecond laser ablation in deionized water[134, 135, 200] as mobile Surface Enhanced Raman Scattering (SERS) probes for the identification of biological species at ultra-low concentrations. First, we found that these core-shells can strongly enhance Raman signals from R6G molecules even if the Si content of the shell exceeds 70%.[135] Using such contamination-free SERS nanoprobes, we demonstrated successful identification of ultra-low concentrations of 2 types of bacteria (Listeria innocua and Escherichia coli),[135] as well as the identification of critically important spoilage yeast cultures in food products[149]. The obtained results promise more compatible SERS probes based on contamination-free laser-synthesized nanomaterials with Si shell surfaces.

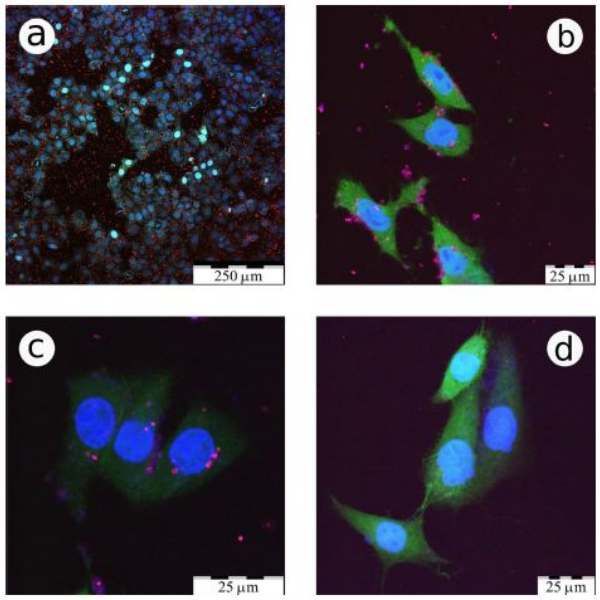

Figure 18. *Confocal fluorescence microscopy images of CF2Th cancer cells incubated with laser-synthesized nanoparticles (red-pink-violet) under different magnification scales (a,b,c) and that of a control sample without nanoparticles (d). Panel (c) presents the cells after washing out of nanoparticles from extracellular space. Cell nuclei and cytoplasm are colored blue and green, respectively. Adapted from Ref. 13 with permission under a Creative Commons CC-BY license.*

Photodynamic Therapy. Photodynamic therapy (PDT) is a promising approach to cancer treatment that is relatively noninvasive with limited systemic toxicity. In PDT, a photosensitizer is activated by light, then transfers energy from its electronically excited triplet state energy to nearby oxygen molecules. This energy transfer produces reactive singlet oxygen ($^1O_2$) that kills the cancerous cells. Clinical applications of PDT are often limited by shortcomings of the organic photosensitizing agent with poor water dispersibility, susceptibility to photobleaching and poor biocompatibility. Silicon-based nanoparticles can be superior to organic photosensitizers in terms of photostability and water dispersability. In addition, their luminescence, biodegradability, biocompatibility, and ability to generate $^1O_2$ under visible and near infra-red illumination, make silicon nanoparticles good candidates as photosensitizers for PDT.

We used laser ablation in liquids to prepare silicon nanoparticles that can act as photosensitizers, producing $^1O_2$ and killing microbes, demonstrating potential for antiseptic or disinfectant therapies.[128] The colloidal silicon nanoparticles of well-defined dimension were produced by femtosecond laser ablation in a clean, contamination-free aqueous environment, which eliminates the toxicity problem of alternative fabrication techniques and provides complete sterilization of the resulting product. The Si nanoparticles are capable of generating singlet oxygen ($^1O_2$) upon laser irradiation at various wavelengths and present no photobleaching, which makes them very useful as potential photosensitizers for therapeutic, antiseptic, or disinfection tasks.

RF Thermal Therapy. The capability of radio frequency (**RF**) radiation to heat tissues has been studied in many works, and in the case of cancer this heating can lead to a partial necrosis of tumors.[201] The efficiency of RF-based treatment can be much enhanced by employing electrically-conductive nanosensitizers, such as carbon nanotubes[202] or gold nanoparticles[203]. These nanostructures are normally delivered into the tumor and then heated by RF radiation to selectively destroy cancer cells. However, carbon nanotubes and gold nanoparticles are not biodegradable, which can give rise to long-term accumulation in the body and related toxicity effects.[204]

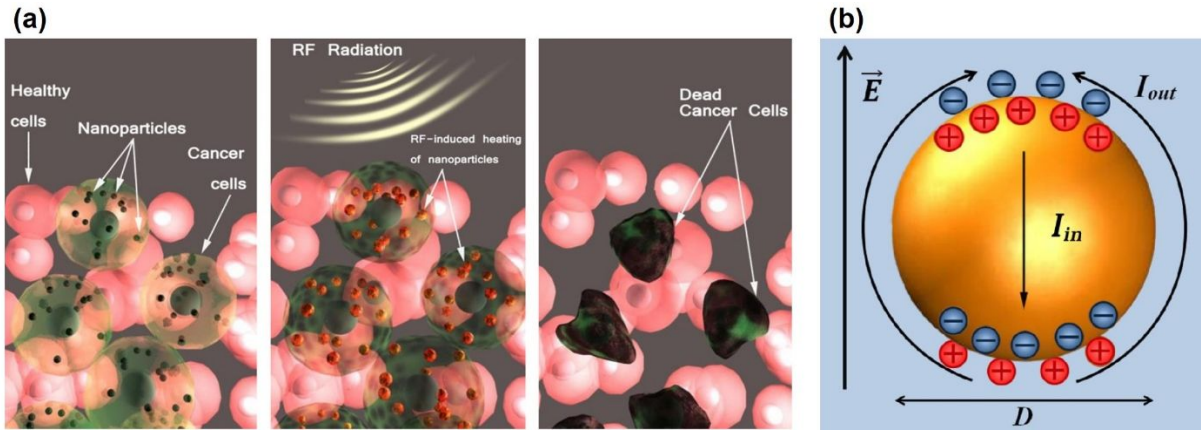

Figure 19. *(a) Schematic representation of RF radiation-induced cancer treatment. nanoparticles are selectively accumulated in tumor cells and are heated, giving rise to selective death of cancer cells, (b) Distribution of electric field around a nanoparticle immersed in a liquid electrolyte under its illumination by RF irradiation. The heating is caused by the ion movement around the nanoparticles due the appearance of electrical double layer at the nanoparticles in response to its RF induced sphere polarization. Adapted from Ref. 30 with permission under a Creative Commons CC-BY license.*

We recently showed that laser-synthesized Si nanoparticles can serve as efficient sensitizers of RF-induced hyperthermia despite their low conductivity, while the efficiency of such therapy was comparable to or better than that of Au nanoparticles.[30] The observed sensitizing effect can be explained by the generation of electrical currents at the nanoparticle/water interface, leading to Joule heating (Figure 19). We recorded efficient RF-induced heating of aqueous dispersions of Si nanoparticles to temperatures above 45-50^{o}C using relatively low nanoparticle concentrations (1

mg/mL). Here, laser-synthesized Si nanoparticles showed much better sensitizing properties compared to porous Si-based counterparts for all used concentrations. *In vivo* experiments confirmed that Si nanoparticles could serve as sensitizers of RF radiation heating to strongly inhibit the growth of carcinoma tumors (Figure 20).

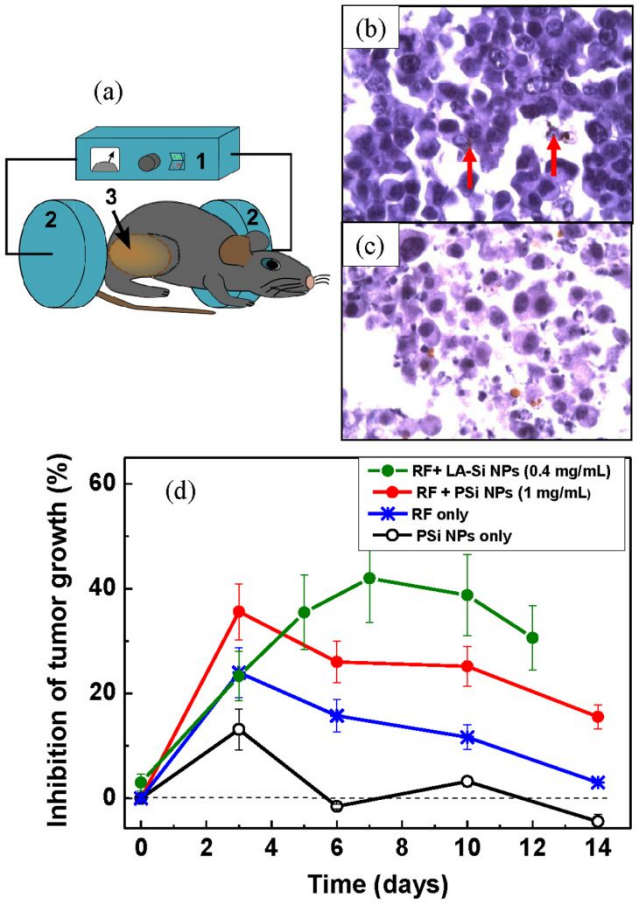

Figure 20. *(a) Schematics of experimental setup for RF-induced therapy. (1) and (2) represent RF radiation source electrodes, respectively, while a tumor area in a mouse is depicted in (3). (b,c) present histological investigation of the tumor 1 hour and 3 days after RF-based treatment, respectively. Cancer cells are identified as dark blue spots, while agglomerations of nanoparticles are depicted by red arrows. (d) Tumor growth inhibition after the injection of Si nanoparticles suspension (black curve); after 2 min treatment of tumor area by RF irradiation (blue); Red and green curves show tumor growth inhibition after the injection of porous Si nanoparticles (0.5 mL, 1 mg/mL) and laser-synthesized Si nanoparticles (0.2 mL, 0.4 mg/mL), respectively, followed by 2 min RF irradiation treatment. From Ref. 30, used with permission under a Creative Commons CC-BY license.*

It should be also noted that laser-ablative synthesis renders possible the synthesis of hybrid SiO_x/Si - graphene oxide nanocomposites, which also look as promising sensitizers for thermal therapies.[205]

Challenges and Opportunities for Laser-Processed Nanosilicon.

As demonstrated in the preceding pages, laser-processed nanosilicon is an extremely promising material for numerous applications, particularly in the biomedical realm. It can combine exceptional purity, which is nearly unachievable with porous silicon or other nanostructures prepared by conventional wet chemical or electrochemical synthesis routes. It offers a multitude of intrinsic properties, which can provide excellent opportunities for the advancement of various applications in energy and healthcare.

For biomedical applications, laser-processed nanosilicon can offer a combination of excellent biocompatibility and biodegradability in the absence of any toxic contamination, which is rather unusual among inorganic materials, as well as a series of outstanding chemical and optical properties that enable promising imaging, therapy, and drug delivery functionalities. Of particular importance, we envision applications of laser-synthesized nanosilicon in cancer theranostics.[206]

For photodetectors, solar cells, and optoelectronics applications, “dry” laser-processed silicon could offer compatibility with the silicon processing technology that forms the basis for microelectronics, which promises easy scaling up of nanosilicon-based devices.

Current challenges include the optimization of different laser processing technologies to match the requirements of nanosilicon for particular applications. In biomedical imaging applications that rely upon the photoluminescence of nanosilicon (Si QDs), surface passivation is required to stabilize the photoluminescence. For many bioapplications, additional encapsulation and/or surface functionalization may be required to achieve targeting of specific cells or tissues. However,

the most effective means of surface passivation, encapsulation, and targeting may protect the silicon nanoparticle so well that it does not degrade *in vivo*. Thus, strategies that combine desirable optical and chemical properties while still allowing the nanosilicon to degrade and be excreted after serving its purpose, must be further developed and optimized.

In many energy-related applications, production cost can be a barrier to scaling and commercialization of laser-processed nanosilicon. Production of high-purity nanosilicon requires high purity precursors, whether solid silicon targets or electronic grade silane or other gases. In optoelectronic applications, where the quantity of nanosilicon per device area is very small, this may not be an issue. However, in applications such as lithium ion batteries and hydrogen generation from water, for which much larger quantities of material are needed, both the high cost of precursors and the relatively low throughput of most currently-available laser-based processes present major challenges.

We envision several pathways for further advancement of laser-processed nanosilicon, from the improvement of laser processing technology and protocols for post-fabrication treatment and functionalization, to the extension and enhancement of functionalities related to projected applications. We believe that the potential of laser-assisted synthesis is not yet fully exploited and one can still profit from the particular conditions of silicon nanostructuring offered by laser processing. Some promising future directions are highlighted in the following brief subsections.

Multifunctional and Nonequilibrium Materials

One promising approach is based on a combination of nanosilicon with other materials *via* doping or formation of composites, which could enhance nanosilicon properties or combine them with other functionalities (*e.g.* magnetic, plasmonic, optical, or photochemical properties). In this sense, traditional wet methods of synthesis, including porous silicon technology and colloidal chemistry,

have serious limitations, as these methods imply the production of nanoformulations from complex compounds under fixed conditions. Laser synthesis is based on quite different (mainly physical) mechanisms for nanostructuring that are not subject to many of the limitations of slower processes that occur closer to equilibrium states. The very rapid initiation and quenching of particle formation in the various laser processing approaches can allow trapping of non-equilibrium states and compositions (*e.g.* hyperdoped materials with dopant concentrations exceeding the solid solubility limit).[207] This makes laser processing a flexible tool for the fabrication of such doped or composite structures.

Multiscale Modeling and Materials Informatics

Design and fabrication of multicomponent nanosilicon formulations with optimized multifunctionality could be greatly accelerated by the effective use of multiscale modeling and materials informatics. Combining multiscale modeling and rapidly maturing tools of materials informatics can facilitate the rapid optimization of composition, structure, and interfaces to achieve desired properties, especially in multicomponent, multifunctional structures. Multiscale modeling adopts different treatments of interactions at different length scales and time scales. For example, local chemical interactions involving up to a few hundred atoms can be treated fully quantum mechanically (QM), while weaker, longer length scale interactions are described by molecular mechanics (MM). The surroundings (*e.g.* solvent) can be treated as a dielectric polarizable continuum. In this framework, optical responses, which are often of greatest interest for nanosilicon applications, can be extracted using density matrix-based time-dependent density functional theory (TDDFT) in the time domain.

Materials informatics combines computational, statistical, and machine learning approaches to predict and optimize composition, structure, and processing of materials to achieve desired

properties and to accelerate the creation and adoption of new materials. Within this framework, results of both conventional experiments and high-throughput methods can be integrated with computational and simulation studies in a machine learning paradigm. Experimental data, physicochemical modeling, and statistical approaches are integrated to generate insights that would elude conventional approaches. Materials informatics can also be used design sets of physical or computational experiments that will maximize information content of each additional data point or data set. These approaches can be extended to automatically conduct sequences of experiments. Greater integration of multiscale modeling and materials informatics could enable discovery and production of laser-processed silicon-containing nanostructures with new combinations of properties.

Quantum Applications

Another promising direction is the creation of quantum materials, which are hierarchically nanostructured hybrids in which quantum communication between different domains and quantum entanglement can be manipulated. Coupled quantum dots in silicon have been extensively explored for creating qubits based on a single isolated electron spin per quantum dot, as in the recent work by Mi *et al.*[208] and many references cited therein. However, such studies all employ lithographic patterning and application of potentials to isolate small domains within a silicon device, such that these domains behave as quantum dots. Charge carriers are confined in these dots by applied potential rather than the fully material-based confinement characteristic of freestanding (or colloidal) quantum dots. Achieving the level of synthetic control required to exploit quantum effects in freestanding coupled quantum dots produced by laser processing is a daunting task, but one worth pursuing.

An example of such coupled quantum dots could be hierarchically structured and topologically controlled multiphase nanoparticles generated by co-ablating multiple targets in a surrounding gaseous or liquid phase. For this, manipulation of the laser wavelength, pulse width, fluence, and surrounding medium together with appropriate target motion could be used to produce a mixed phase (alloyed), core-multiple shells, or multidomain (*e.g.* dumbbell-like) structures with controlled interdomain interactions. These hierarchical quantum materials can provide single photon sources and can contribute to advances in spintronics. Their applications in quantum information processing could include quantum key distribution, quantum networks, and photonic quantum computing.

Nonlinear Multiphoton Imaging

Our work has also shown that laser-processed nanosilicon can exhibit strong two- and three-photon excited luminescence (nonlinear upconversion) which can be suitable for multiphoton microscopy.[209] In that study, 1-photon excitation at 339 nm, two-photon excitation at 778 nm, and three-photon excitation at 1335 nm produced nearly identical photoluminescence, in terms of both spectrum and lifetimes, with peak emission near 650 nm. Suitable wavelengths for two- and three-photon excitation fall in the first and second windows of biological transparency, providing the possibility of relatively deep tissue penetration combined with the three-dimensional imaging capability of multiphoton microscopy. Chandra *et al.* demonstrated two-photon excited confocal microscopy using nanosilicon prepared by a complex multi-step process that yielded particles with peak PL emission at 918 nm.[210] They excited their nanosilicon with a Ti:sapphire laser at 800 nm, and detected the short wavelength tail of the PL below 650 nm. Kharin *et al.* recently demonstrated dual-mode bioimaging based on two-photon emission luminescence (TPEL) and second-harmonic

generation (SHG) channels, using relatively large (10-30 nm) laser-synthesized nanoparticles, that did not exhibit photoluminescence from quantum-confined excitonic states.[211] They also showed that non-linear response of these large nanoparticles exceeded that of smaller ones (< 5 nm), while the combination of TPEL and SHG channels enabled efficient tracing of both separated Si NPs and their aggregations in different cell compartments.[211] The obtained bi-modal contrast provides a previously-lacking imaging functionality for large Si NPs as efficient sensitizers for RF-induced (see Paragraph 3.3.3.2) and other therapies. In general, the potential of nanosilicon for multi-photon excited imaging has begun to be explored, but neither the materials nor microscopy systems has been optimized, and the full potential of this imaging approach remains to be tapped. As one of promising avenues, we see the addition of a polarizable Ge component to enhance the multiphoton absorbance cross-section and shift the emission wavelength to the second window of biological optical transparency to enable high-contrast deep tissue imaging. We have demonstrated the direct production of silicon-germanium alloy nanoparticles by laser pyrolysis of silane-germane mixtures,[212, 213] but the nonlinear optical properties of these group IV alloy nanoparticles remain to be optimized and exploited for imaging.

Nanosilicon for Delivery of Nuclear Medicine

Nuclear nanomedicine exploits the ability of nanocarriers to endow radionuclides with tumor targeting ability and high loading capacity along with enhanced retention to avoid rapid clearance that is typical of molecular radiopharmaceuticals. Thus, nuclear nanomedicine has great potential to treat tumors and metastases. Despite these promises, progress in this field has been somewhat slow, primarily due to a lack of safe and excretable nanocarriers that also have favorable pharmacokinetics to efficiently deliver and retain radionuclides in a tumor. We recently introduced biodegradable laser-synthesized Si nanoparticles with high chemical purity, round shape,

controllable size, and narrow size distribution as carriers of the therapeutic ^{188}Re radionuclide.[214] Only one hour was required for conjugation of the PEG-coated Si nanostructures with radioactive ^{188}Re, which is substantially shorter than the ^{188}Re half-life of 17 hours. Upon intravenous administration in a Wistar rat model, the conjugates circulated freely in the blood stream to reach all organs and the target tumors. The observed biodistribution was dramatically different from that of ^{188}Re salt, which mostly accumulates in the thyroid gland. The nanoparticle-based delivery also ensured excellent retention of ^{188}Re in the tumor, again in contrast to the salt, which maximizes the therapeutic effect. Ultimately, the radionuclide nanocarrier exhibited complete time-delayed bioelimination. Tests of rat survival in this study showed excellent therapeutic effect, with 72% of treated rats surviving, while 0% of untreated control animals survived. This strategy of creating a nanosilicon-based biodegradable complex for radionuclide delivery could be a major step forward in nuclear nanomedicine.

Engineering for Scale-Up

We believe that straightforward engineering approaches can be applied to scale up most laser-processing methods and reduce costs of production for applications where that is a key limitation. Nearly all studies of laser-processed nanosilicon to date have been aimed at understanding material properties or achieving proof-of-concept demonstrations of particular applications. For most of these processing approaches, serious attempts at scale-up have not yet been made. Thus, there is tremendous room for work in this direction as demand for laser-synthesized silicon increases. For examples, laser pyrolysis processes described in this paper have mainly been done using lasers of up to 100 W to produce up to 1 g/h of nanosilicon. However, CO_2 lasers are available at powers up to many kW, and laser pyrolysis processes, in general, have been scaled to kg/h volumes, which would be sufficient for many applications.

Acknowledgements:

A. V. K. and I. N. Z. acknowledge contribution of Russian Science Foundation (Project 19-72-30012) for access to some databases and travel exchange support. A. V. K., I. N. Z and P. N. P. are also grateful to MEPhI Academic Excellence Project (Contract No. 02.a03.21.0005). This paper is dedicated to our co-author, Dr. Ajay Singh, who unexpectedly passed away on October 20, 2018.

References

1. Hull, R., *Properties of Crystalline Silicon*. Institution of Electrical Engineers: London, 2006; 1016 p.

2. Carlisle, E. M., Silicon: A Requirement in Bone Formation Independent of Vitamin D1. *Calcif Tissue Int* **1981,** *33*, 27-34.

3. Jugdaohsingh, R., Silicon and Bone Health. *J Nutr Health Aging* **2007,** *11*, 99-110.

4. Emerick, R. J.; Kayongo-Male, H., Interactive Effects of Dietary Silicon, Copper, and Zinc in the Rat. *J Nutr Biochem* **1990,** *1*, 35-40.

5. Park, J. H.; Gu, L.; von Maltzahn, G.; Ruoslahti, E.; Bhatia, S. N.; Sailor, M. J., Biodegradable Luminescent Porous Silicon Nanoparticles for *In Vivo* Applications. *Nat Mater* **2009,** *8*, 331-336.

6. Baati, T.; Al-Kattan, A.; Esteve, M. A.; Njim, L.; Ryabchikov, Y.; Chaspoul, F.; Hammami, M.; Sentis, M.; Kabashin, A. V.; Braguer, D., Ultrapure Laser-Synthesized Si-Based Nanomaterials for Biomedical Applications: *In Vivo* Assessment of Safety and Biodistribution. *Sci Rep* **2016,** *6*, 25400.

7. Steigerwald, M. L.; Brus, L. E., Synthesis, Stabilization, and Electronic-Structure of Quantum Semiconductor Nanoclusters. *Annu Rev Mater Sci* **1989,** *19*, 471-495.

8. Canham, L. T., Silicon Quantum Wire Array Fabrication by Electrochemical and Chemical Dissolution of Wafers. *Appl Phys Lett* **1990,** *57*, 1046-1048.

9. Takagi, H.; Ogawa, H.; Yamazaki, Y.; Ishizaki, A.; Nakagiri, T., Quantum Size Effects on Photoluminescence in Ultrafine Si Particles. *Appl Phys Lett* **1990,** *56*, 2379-2380.

10. Soref, R. A., Silicon-Based Optoelectronics. *P IEEE* **1993,** *81*, 1687-1706.

11. Erogbogbo, F.; Yong, K. T.; Roy, I.; Xu, G. X.; Prasad, P. N.; Swihart, M. T., Biocompatible Luminescent Silicon Quantum Dots for Imaging of Cancer Cells. *ACS Nano* **2008,** *2*, 873-878.

12. Gu, L.; Hall, D. J.; Qin, Z. T.; Anglin, E.; Joo, J.; Mooney, D. J.; Howell, S. B.; Sailor, M. J., *In Vivo* Time-Gated Fluorescence Imaging with Biodegradable Luminescent Porous Silicon Nanoparticles. *Nat Commun* **2013,** *4*, 2326.

13. Gongalsky, M. B.; Osminkina, L. A.; Pereira, A.; Manankov, A. A.; Fedorenko, A. A.; Vasiliev, A. N.; Solovyev, V. V.; Kudryavtsev, A. A.; Sentis, M.; Kabashin, A. V.; Timoshenko, V. Y., Laser-Synthesized Oxide-Passivated Bright Si Quantum Dots for Bioimaging. *Sci Rep* **2016,** *6*, 24732.

14. Jansen, H.; Deboer, M.; Legtenberg, R.; Elwenspoek, M., The Black Silicon Method - a Universal Method for Determining the Parameter Setting of a Fluorine-Based Reactive Ion Etcher in Deep Silicon Trench Etching with Profile Control. *J Micromech Microeng* **1995,** *5*, 115-120.

15. Her, T. H.; Finlay, R. J.; Wu, C.; Deliwala, S.; Mazur, E., Microstructuring of Silicon with Femtosecond Laser Pulses. *Appl Phys Lett* **1998,** *73*, 1673-1675.

16. Wu, C.; Crouch, C. H.; Zhao, L.; Mazur, E., Visible Luminescence from Silicon Surfaces Microstructured in Air. *Appl Phys Lett* **2002,** *81*, 1999-2001.

17. Kim, H.; Han, B.; Choo, J.; Cho, J., Three-Dimensional Porous Silicon Particles for Use in High-Performance Lithium Secondary Batteries. *Angew Chem, Int Edit* **2008,** *47*, 10151-10154.

18. Kim, H.; Seo, M.; Park, M. H.; Cho, J., A Critical Size of Silicon Nano-Anodes for Lithium Rechargeable Batteries. *Angew Chem, Int Edit* **2010,** *49*, 2146-2149.

19. Chan, C. K.; Peng, H. L.; Liu, G.; McIlwrath, K.; Zhang, X. F.; Huggins, R. A.; Cui, Y., High-Performance Lithium Battery Anodes Using Silicon Nanowires. *Nat Nanotechnol* **2008,** *3*, 31-35.

20. Cui, L. F.; Ruffo, R.; Chan, C. K.; Peng, H. L.; Cui, Y., Crystalline-Amorphous Core-Shell Silicon Nanowires for High Capacity and High Current Battery Electrodes. *Nano Lett* **2009,** *9*, 491-495.

21. Litvinenko, S.; Alekseev, S.; Lysenko, V.; Venturello, A.; Geobaldo, F.; Gulina, L.; Kuznetsov, G.; Tolstoy, V.; Skryshevsky, V.; Garrone, E.; Barbier, D., Hydrogen Production from Nano-Porous Si Powder Formed by Stain Etching. *Int J Hydrogen Energ* **2010,** *35*, 6773-6778.

22. Bahruji, H.; Bowker, M.; Davies, P. R., Photoactivated Reaction of Water with Silicon Nanoparticles. *Int J Hydrogen Energ* **2009,** *34*, 8504-8510.

23. Erogbogbo, F.; Lin, T.; Tucciarone, P. M.; LaJoie, K. M.; Lai, L.; Patki, G. D.; Prasad, P. N.; Swihart, M. T., On-Demand Hydrogen Generation Using Nanosilicon: Splitting Water without Light, Heat, or Electricity. *Nano Lett* **2013,** *13*, 451-456.

24. Vaccari, L.; Canton, D.; Zaffaroni, N.; Villa, R.; Tormen, M.; di Fabrizio, E., Porous Silicon as Drug Carrier for Controlled Delivery of Doxorubicin Anticancer Agent. *Microelectron Eng* **2006,** *83*, 1598-1601.

25. Salonen, J.; Kaukonen, A. M.; Hirvonen, J.; Lehto, V. P., Mesoporous Silicon in Drug Delivery Applications. *J Pharm Sci-Us* **2008,** *97*, 632-653.

26. Kovalev, D.; Gross, E.; Kunzner, N.; Koch, F.; Timoshenko, V. Y.; Fujii, M., Resonant Electronic Energy Transfer from Excitons Confined in Silicon Nanocrystals to Oxygen Molecules. *Phys Rev Lett* **2002,** *89* 137401.

27. Kovalev, D.; Fujii, M., Silicon Nanocrystals: Photosensitizers for Oxygen Molecules. *Adv Mater* **2005,** *17*, 2531-2544.

28. Timoshenko, V. Y.; Kudryavtsev, A. A.; Osminkina, L. A.; Vorontsov, A. S.; Ryabchikov, Y. V.; Belogorokhov, I. A.; Kovalev, D.; Kashkarov, P. K., Silicon Nanocrystals as Photosensitizers of Active Oxygen for Biomedical Applications. *JETP Lett - USSR* **2006,** *83*, 423-426.

29. Lee, C.; Kim, H.; Hong, C.; Kim, M.; Hong, S. S.; Lee, D. H.; Lee, W. I., Porous Silicon as an Agent for Cancer Thermotherapy Based on Near-Infrared Light Irradiation. *J Mater Chem* **2008,** *18*, 4790-4795.

30. Tamarov, K. P.; Osminkina, L. A.; Zinovyev, S. V.; Maximova, K. A.; Kargina, J. V.; Gongalsky, M. B.; Ryabchikov, Y.; Al-Kattan, A.; Sviridov, A. P.; Sentis, M.; Ivanov, A. V.; Nikiforov, V. N.; Kabashin, A. V.; Timoshenko, V. Y., Radio Frequency Radiation-Induced Hyperthermia Using Si Nanoparticle-Based Sensitizers for Mild Cancer Therapy. *Sci Rep* **2014,** *4*, 7034.

31. Sviridov, A. P.; Andreev, V. G.; Ivanova, E. M.; Osminkina, L. A.; Tamarov, K. P.; Timoshenko, V. Y., Porous Silicon Nanoparticles as Sensitizers for Ultrasonic Hyperthermia. *Appl Phys Lett* **2013,** *103*, 193110.

32. He, Y., *Silicon Nano-Biotechnology*. Springer: Heidelberg, 2014;109 pages.

33. Sailor, M. J., Porous Silicon in Practice Preparation, Characterization and Applications. Wiley-VCH,: Weinheim, 2012; 249 pages.

34. Santos, H. A., *Porous Silicon for Biomedical Applications*. Elsevier/Woodhead Publishing: Amsterdam, 2014; 526 pages.

35. English, D. S.; Pell, L. E.; Yu, Z. H.; Barbara, P. F.; Korgel, B. A., Size Tunable Visible Luminescence from Individual Organic Monolayer Stabilized Silicon Nanocrystal Quantum Dots. *Nano Lett* **2002,** *2*, 681-685.

36. Neiner, D.; Chiu, H. W.; Kauzlarich, S. M., Low-Temperature Solution Route to Macroscopic Amounts of Hydrogen Terminated Silicon Nanoparticles. *J Am Chem Soc* **2006,** *128*, 11016-11017.

37. Zhang, X. M.; Neiner, D.; Wang, S. Z.; Louie, A. Y.; Kauzlarich, S. M., A New Solution Route to Hydrogen-Terminated Silicon Nanoparticles: Synthesis, Functionalization and Water Stability. *Nanotechnology* **2007,** *18*, 95601.

38. Tilley, R. D.; Yamamoto, K., The Microemulsion Synthesis of Hydrophobic and Hydrophilic Silicon Nanocrystals. *Adv Mater* **2006,** *18*, 2053-2056.

39. Shirahata, N.; Furumi, S.; Sakka, Y., Micro-Emulsion Synthesis of Blue-Luminescent Silicon Nanoparticles Stabilized with Alkoxy Monolayers. *J Cryst Growth* **2009,** *311*, 634-637.

40. Holmes, J. D.; Ziegler, K. J.; Doty, R. C.; Pell, L. E.; Johnston, K. P.; Korgel, B. A., Highly Luminescent Silicon Nanocrystals with Discrete Optical Transitions. *J Am Chem Soc* **2001,** *123*, 3743-3748.

41. Hessel, C. M.; Reid, D.; Panthani, M. G.; Rasch, M. R.; Goodfellow, B. W.; Wei, J.; Fujii, H.; Akhavan, V.; Korgel, B. A., Synthesis of Ligand-Stabilized Silicon Nanocrystals with Size-Dependent Photoluminescence Spanning Visible to Near-Infrared Wavelengths. *Chem Mater* **2012,** *24*, 393-401.

42. Hessel, C. M.; Henderson, E. J.; Veinot, J. G. C., Hydrogen Silsesquioxane: A Molecular Precursor for Nanocrystalline Si−SiO_2 Composites and Freestanding Hydride-Surface-Terminated Silicon Nanoparticles. *Chem Mater* **2006,** *18*, 6139-6146.

43. Zhong, Y.; Peng, F.; Bao, F.; Wang, S.; Ji, X.; Yang, L.; Su, Y.; Lee, S.-T.; He, Y., Large-Scale Aqueous Synthesis of Fluorescent and Biocompatible Silicon Nanoparticles and Their Use as Highly Photostable Biological Probes. *J Am Chem Soc* **2013,** *135*, 8350-8356.

44. Pujari, S. P.; Driss, H.; Bannani, F.; van Lagen, B.; Zuilhof, H., One-Pot Gram-Scale Synthesis of Hydrogen-Terminated Silicon Nanoparticles. *Chem Mater* **2018,** *30*, 6503-6512.

45. Dhas, N. A.; Raj, C. P.; Gedanken, A., Preparation of Luminescent Silicon Nanoparticles: A Novel Sonochemical Approach. *Chem Mater* **1998,** *10*, 3278- 3281 .

46. Heintz, A. S.; Fink, M. J.; Mitchell, B. S., Mechanochemical Synthesis of Blue Luminescent Alkyl/Alkenyl-Passivated Silicon Nanoparticles. *Adv Mater* **2007,** *19*, 3984- 3988.

47. Sangghaleh, F.; Sychugov, I.; Yang, Z. Y.; Veinot, J. G. C.; Linnros, J., Near-Unity Internal Quantum Efficiency of Luminescent Silicon Nanocrystals with Ligand Passivation. *ACS Nano* **2015,** *9*, 7097-7104.

48. Sugimoto, H.; Fujii, M.; Imakita, K.; Hayashi, S.; Akamatsu, K., Codoping *n*- and *p*-Type Impurities in Colloidal Silicon Nanocrystals: Controlling Luminescence Energy from Below Bulk Band Gap to Visible Range. *J Phys Chem C* **2013,** *117*, 11850-11857.

49. Fojtik, A.; Weller, H.; Fiechter, S.; Henglein, A., Preparation of Colloidal Silicon and Preliminary Photochemical Experiments. *Chem Phys Lett* **1987,** *134*, 477-479.

50. Fojtik, A.; Henglein, A., Luminescent Colloidal Silicon Particles. *Chem Phys Lett* **1994,** *221*, 363-367.

51. Wu, J. J.; Flagan, R. C., Onset of Runaway Nucleation in Aerosol Reactors. *J Appl Phys* **1987,** *61*, 1365-1371.

52. Gupta, A.; Swihart, M. T.; Wiggers, H., Luminescent Colloidal Dispersion of Silicon Quantum Dots from Microwave Plasma Synthesis: Exploring the Photoluminescence Behavior across the Visible Spectrum. *Adv Funct Mater* **2009,** *19*, 696-703.

53. Mangolini, L.; Thimsen, E.; Kortshagen, U., High-Yield Plasma Synthesis of Luminescent Silicon Nanocrystals. *Nano Lett* **2005,** *5*, 655-659.

54. Kortshagen, U., Nonthermal Plasma Synthesis of Semiconductor Nanocrystals. *J Phys D Appl Phys* **2009,** *42*, 113001.

55. Mangolini, L.; Kortshagen, U., Plasma-Assisted Synthesis of Silicon Nanocrystal Inks. *Adv Mater* **2007,** *19*, 2513-2519.

56. Okada, R.; Iijima, S., Oxidation Property of Silicon Small Particles. *Appl Phys Lett* **1991,** *58*, 1662-1663.

57. Dimaria, D. J.; Kirtley, J. R.; Pakulis, E. J.; Dong, D. W.; Kuan, T. S.; Pesavento, F. L.; Theis, T. N.; Cutro, J. A.; Brorson, S. D., Electroluminescence Studies in Silicon Dioxide Films Containing Tiny Silicon Islands. *J Appl Phys* **1984,** *56*, 401-416.

58. Berger, S.; Schachter, L.; Tamir, S., Photoluminescence as a Surface-Effect in Nanostructures. *Nanostruct Mater* **1997,** *8*, 231-242.

59. Islam, M. A.; Sinelnikov, R.; Howlader, M. A.; Faramus, A.; Veinot, J. G. C., Mixed Surface Chemistry: An Approach to Highly Luminescent Biocompatible Amphiphilic Silicon Nanocrystals. *Chem Mater* **2018,** *30*, 8925-8931.

60. Koynov, S.; Pereira, R. N.; Crnolatac, I.; Kovalev, D.; Huygens, A.; Chirvony, V.; Stutzmann, M.; de Witte, P., Purification of Nano-Porous Silicon for Biomedical Applications. *Adv Eng Mater* **2011,** *13*, B225-B233.

61. Dasog, M.; De los Reyes, G. B.; Titova, L. V.; Hegmann, F. A.; Veinot, J. G. C., Size Vs Surface: Tuning the Photoluminescence of Freestanding Silicon Nanocrystals across the Visible Spectrum *via* Surface Groups. *ACS Nano* **2014,** *8*, 9636-9648.

62. Dasog, M.; Kehrle, J.; Rieger, B.; Veinot, J. G. C., Silicon Nanocrystals and Silicon-Polymer Hybrids: Synthesis, Surface Engineering, and Applications. *Angew Chemie Int Edit* **2016,** *55*, 2322-2339.

63. Höhlein, I. M. D.; Angı, A.; Sinelnikov, R.; Veinot, J. G. C.; Rieger, B., Functionalization of Hydride-Terminated Photoluminescent Silicon Nanocrystals with Organolithium Reagents. *Chem – Eur J* **2015,** *21*, 2755-2758.

64. Angı, A.; Sinelnikov, R.; Meldrum, A.; Veinot, J. G. C.; Balberg, I.; Azulay, D.; Millo, O.; Rieger, B., Photoluminescence through in-Gap States in Phenylacetylene Functionalized Silicon Nanocrystals. *Nanoscale* **2016,** *8*, 7849-7853.

65. Wolf, O.; Dasog, M.; Yang, Z.; Balberg, I.; Veinot, J. G. C.; Millo, O., Doping and Quantum Confinement Effects in Single Si Nanocrystals Observed by Scanning Tunneling Spectroscopy. *Nano Lett* **2013,** *13*, 2516-2521.

66. Cheng, X.; Lowe, S. B.; Reece, P. J.; Gooding, J. J., Colloidal Silicon Quantum Dots: From Preparation to the Modification of Self-Assembled Monolayers (SAMs) for Bio-Applications. *Chem Soc Rev* **2014,** *43*, 2680-2700.

67. Nishikawa, H.; Shiroyama, T.; Nakamura, R.; Ohki, Y.; Nagasawa, K.; Hama, Y., Photoluminescence from Defect Centers in High-Purity Silica Glasses Observed under 7.9-eV Excitation. *Phys Rev B* **1992,** *45*, 586-591.

68. Rebohle, L.; von Borany, J.; Fröb, H.; Skorupa, W., Blue Photo- and Electroluminescence of Silicon Dioxide Layers Ion-Implanted with Group IV Elements. *Appl Phys B* **2000,** *71*, 131-151.

69. Dasog, M.; Yang, Z.; Regli, S.; Atkins, T. M.; Faramus, A.; Singh, M. P.; Muthuswamy, E.; Kauzlarich, S. M.; Tilley, R. D.; Veinot, J. G. C., Chemical Insight into the Origin of Red and Blue Photoluminescence Arising from Freestanding Silicon Nanocrystals. *Acs Nano* **2013,** *7*, 2676-2685.

70. Delerue, C.; Lannoo, M.; Allan, G., Excitonic and Quasiparticle Gaps in Si Nanocrystals. *Phys Rev Lett* **2000,** *84*, 2457-2460.

71. Wolkin, M. V.; Jorne, J.; Fauchet, P. M.; Allan, G.; Delerue, C., Electronic States and Luminescence in Porous Silicon Quantum Dots: The Role of Oxygen. *Phys Rev Lett* **1999,** *82*, 197-200.

72. Kovalev, D.; Heckler, H.; Polisski, G.; Diener, J.; Koch, F., Optical Properties of Silicon Nanocrystals. *Opt Mater* **2001,** *17*, 35-40.

73. Kabashin, A. V.; Delaporte, P.; Pereira, A.; Grojo, D.; Torres, R.; Sarnet, T.; Sentis, M., Nanofabrication with Pulsed Lasers. *Nanoscale Res Lett* **2010,** *5*, 454-463.

74. Cannon, W. R.; Danforth, S. C.; Haggerty, J. S.; Marra, R. A., Sinterable Ceramic Powders from Laser-Driven Reactions 2. Powder Characteristics and Process Variables. *J Am Ceram Soc* **1982,** *65*, 330-335.

75. Cannon, W. R.; Danforth, S. C.; Flint, J. H.; Haggerty, J. S.; Marra, R. A., Sinterable Ceramic Powders from Laser-Driven Reactions .1. Process Description and Modeling. *J Am Ceram Soc* **1982,** *65*, 324-330.

76. Fojtik, A.; Henglein, A., Laser Ablation of Films and Suspended Particles in a Solvent - Formation of Cluster and Colloid Solutions. *Ber Bunsen Phys Chem* **1993,** *97*, 252-254.

77. Li, X. G.; He, Y. Q.; Swihart, M. T., Surface Functionalization of Silicon Nanoparticles Produced by Laser-Driven Pyrolysis of Silane Followed by HF-HNO_3 Etching. *Langmuir* **2004,** *20*, 4720-4727.

78. Hua, F. J.; Swihart, M. T.; Ruckenstein, E., Efficient Surface Grafting of Luminescent Silicon Quantum Dots by Photoinitiated Hydrosilylation. *Langmuir* **2005,** *21*, 6054-6062.

79. Pedraza, A. J.; Fowlkes, J. D.; Lowndes, D. H., Silicon Microcolumn Arrays Grown by Nanosecond Pulsed-Excimer Laser Irradiation. *Appl Phys Lett* **1999,** *74*, 2322-2324.

80. Movtchan, I. A.; Marine, W.; Dreyfus, R. W.; Le, H. C.; Sentis, M.; Autric, M., Optical Spectroscopy of Emission from Si-SiO_x Nanoclusters Formed by Laser Ablation. *Appl Surf Sci* **1996,** *96-8*, 251-260.

81. Geohegan, D. B.; Puretzky, A. A.; Duscher, G.; Pennycook, S. J., Photoluminescence from Gas-Suspended SiO_x Nanoparticles Synthesized by Laser Ablation. *Appl Phys Lett* **1998,** *73*, 438-440.

82. Geohegan, D. B.; Puretzky, A. A.; Duscher, G.; Pennycook, S. J., Time-Resolved Imaging of Gas Phase Nanoparticle Synthesis by Laser Ablation. *Appl Phys Lett* **1998,** *72*, 2987-2989.

83. Werwa, E.; Seraphin, A. A.; Chiu, L. A.; Zhou, C. X.; Kolenbrander, K. D., Synthesis and Processing of Silicon Nanocrystallites Using a Pulsed-Laser Ablation Supersonic Expansion Method. *Appl Phys Lett* **1994,** *64*, 1821-1823.

84. Yamada, Y.; Orii, T.; Umezu, I.; Takeyama, S.; Yoshida, T., Optical Properties of Silicon Nanocrystallites Prepared by Excimer Laser Ablation in Inert Gas. *Jpn J Appl Phys 1* **1996,** *35*, 1361-1365.

85. Makimura, T.; Kunii, Y.; Murakami, K., Light Emission from Nanometer-Sized Silicon Particles Fabricated by the Laser Ablation Method. *Jpn J Appl Phys 1* **1996,** *35*, 4780-4784.

86. Makimura, T.; Kunii, Y.; Ono, N.; Murakami, K., Silicon Nanoparticles Embedded in SiO_2 Films with Visible Photoluminescence. *Appl Surf Sci* **1998,** *127*, 388-392.

87. Umezu, I.; Shibata, K.; Yamaguchi, S.; Sugimura, A.; Yamada, Y.; Yoshida, T., Effects of Thermal Processes on Photoluminescence of Silicon Nanocrystallites Prepared by Pulsed Laser Ablation. *J Appl Phys* **1998,** *84*, 6448-6450.

88. Patrone, L.; Nelson, D.; Safarov, V. I.; Sentis, M.; Marine, W.; Giorgio, S., Photoluminescence of Silicon Nanoclusters with Reduced Size Dispersion Produced by Laser Ablation. *J Appl Phys* **2000,** *87*, 3829-3837.

89. Marine, W.; Patrone, L.; Luk'yanchuk, B.; Sentis, M., Strategy of Nanocluster and Nanostructure Synthesis by Conventional Pulsed Laser Ablation. *Appl Surf Sci* **2000,** *154*, 345-352.

90. Suzuki, N.; Makino, T.; Yamada, Y.; Yoshida, T.; Onari, S., Structures and Optical Properties of Silicon Nanocrystallites Prepared by Pulsed-Laser Ablation in Inert Background Gas. *Appl Phys Lett* **2000,** *76*, 1389-1391.

91. Kabashin, A. V.; Charbonneau-Lefort, M.; Meunier, M.; Leonelli, R., Effects of Deposition and Post-Fabrication Conditions on Photoluminescent Properties of Nanostructured Si/SiO_x Films Prepared by Laser Ablation. *Appl Surf Sci* **2000,** *168*, 328-331.

92. Kabashin, A. V.; Meunier, M.; Leonelli, R., Photoluminescence Characterization of Si-Based Nanostructured Films Produced by Pulsed Laser Ablation. *J Vac Sci Technol B* **2001,** *19*, 2217-2222.

93. Kabashin, A. V.; Sylvestre, J. P.; Patskovsky, S.; Meunier, M., Correlation between Photoluminescence Properties and Morphology of Laser-Ablated Si/SiO_x Nanostructured Films. *J Appl Phys* **2002,** *91*, 3248-3254.

94. Kim, J. H.; Jeon, K. A.; Kim, G. H.; Lee, S. Y., Optical Properties of Silicon Nanocrystalline Thin Films Grown by Pulsed Laser Deposition. *Opt Mater* **2005,** *27*, 991-994.

95. Yoshida, T.; Yamada, Y.; Orii, T., Electroluminescence of Silicon Nanocrystallites Prepared by Pulsed Laser Ablation in Reduced Pressure Inert Gas. *J Appl Phys* **1998,** *83*, 5427-5432.

96. Makino, T.; Yamada, Y.; Suzuki, N.; Yoshida, T.; Onari, S., Electroluminescence of Monodispersed Silicon Nanocrystallites Synthesized by Pulsed Laser Ablation in Inert Background Gas. *Appl Surf Sci* **2002,** *197*, 594-597.

97. Ishchenko, A. A.; Fetisov, G. V.; Aslanov, L. A., *Nanosilicon : Properties, Synthesis, Applications, Methods of Analysis and Control*. CRC Press: Boca Raton, Florida, 2014; 755 pages.

98. Mangolini, L.; Kortshagen, U., Selective Nanoparticle Heating: Another Form of Nonequilibrium in Dusty Plasmas. *Phys Rev E* **2009,** *79*, 026405.

99. Seto, T.; Kawakami, Y.; Suzuki, N.; Hirasawa, M.; Aya, N., Laser Synthesis of Uniform Silicon Single Nanodots. *Nano Lett* **2001,** *1*, 315-318.

100. Orii, T.; Hirasawa, M.; Seto, T., Tunable, Narrow-Band Light Emission from Size-Selected Si Nanoparticles Produced by Pulsed-Laser Ablation. *Appl Phys Lett* **2003,** *83*, 3395-3397.

101. Morales, A. M.; Lieber, C. M., A Laser Ablation Method for the Synthesis of Crystalline Semiconductor Nanowires. *Science* **1998,** *279*, 208-211.

102. Zhang, Y. F.; Tang, Y. H.; Wang, N.; Yu, D. P.; Lee, C. S.; Bello, I.; Lee, S. T., Silicon Nanowires Prepared by Laser Ablation at High Temperature. *Appl Phys Lett* **1998,** *72*, 1835-1837.

103. Fukata, N.; Oshima, T.; Murakami, K.; Kizuka, T.; Tsurui, T.; Ito, S., Phonon Confinement Effect of Silicon Nanowires Synthesized by Laser Ablation. *Appl Phys Lett* **2005,** *86*, 213112.

104. Wang, K.; Chung, S. Y.; Kim, D., Morphology of Si Nanowires Fabricated by Laser Ablation Using Gold Catalysts. *Appl Phys A* **2004,** *79*, 895-897.

105. Evlyukhin, A. B.; Reinhardt, C.; Seidel, A.; Luk'yanchuk, B. S.; Chichkov, B. N., Optical Response Features of Si-Nanoparticle Arrays. *Phys Rev B* **2010,** *82*, 045404.

106. Evlyukhin, A. B.; Novikov, S. M.; Zywietz, U.; Eriksen, R. L.; Reinhardt, C.; Bozhevolnyi, S. I.; Chichkov, B. N., Demonstration of Magnetic Dipole Resonances of Dielectric Nanospheres in the Visible Region. *Nano Lett* **2012,** *12*, 3749-3755.

107. Kuznetsov, A. I.; Miroshnichenko, A. E.; Fu, Y. H.; Zhang, J.; Luk'yanchuk, B., Magnetic Light. *Sci Rep* **2012,** *2*, 492.

108. Fu, Y. H.; Kuznetsov, A. I.; Miroshnichenko, A. E.; Yu, Y. F.; Luk'yanchuk, B., Directional Visible Light Scattering by Silicon Nanoparticles. *Nat Commun* **2013,** *4*, 1527.

109. Zywietz, U.; Evlyukhin, A. B.; Reinhardt, C.; Chichkov, B. N., Laser Printing of Silicon Nanoparticles with Resonant Optical Electric and Magnetic Responses. *Nat Commun* **2014,** *5*, 3402.

110. Zywietz, U.; Reinhardt, C.; Evlyukhin, A. B.; Birr, T.; Chichkov, B. N., Generation and Patterning of Si Nanoparticles by Femtosecond Laser Pulses. *Appl Phys A* **2014,** *114*, 45-50.

111. Kabashin, A. V.; Meunier, M., Fabrication of Photoluminescent Si-Based Layers by Air Optical Breakdown near the Silicon Surface. *Appl Surf Sci* **2002,** *186*, 578-582.

112. Kabashin, A. V.; Meunier, M., Visible Photoluminescence from Nanostructured Si-Based Layers Produced by Air Optical Breakdown on Silicon. *Appl Phys Lett* **2003,** *82*, 1619-1621.

113. Kabashin, A. V.; Meunier, M., Laser-Induced Treatment of Silicon in Air and Formation of Si/SiO_x Photoluminescent Nanostructured Layers. *Mat Sci Eng B-Solid* **2003,** *101*, 60-64.

114. Yang, D. Q.; Kabashin, A. V.; Pilon-Marien, V. G.; Sacher, E.; Meunier, M., Optical Breakdown Processing: Influence of the Ambient Gas on the Properties of the Nanostructured Si-Based Layers Formed. *J Appl Phys* **2004,** *95*, 5722-5728.

115. Raĭzer, I. U. P., *Laser-Induced Discharge Phenomena*. Consultants Bureau: New York, 1977; 366 p.

116. Bunkin, F. V.; Konov, V. I.; Prokhoro.Am; Fedorov, V. B., Laser Spark in Slow Combustion Regime. *JETP Lett-USSR* **1969,** *9*, 371-374.

117. Kabashin, A. V.; Nikitin, P. I.; Marine, W.; Sentis, M., Experimental Study of Spontaneous Electric Field Generated by a Laser Plasma. *Appl Phys Lett* **1998,** *73*, 25-27.

118. Kabashin, A. V.; Nikitin, P. I., Electric Fields of a Laser Spark Produced by Radiation with Various Parameters. *Quantum Electron* **1997,** *27*, 536-541.

119. Serov, R.; Richardson, M. C., Measurement of Intense Magnetic-Fields Associated with Laser-Produced Plasmas. *Appl Phys Lett* **1976,** *28*, 115-118.

120. Neddersen, J.; Chumanov, G.; Cotton, T. M., Laser-Ablation of Metals - A New Method for Preparing SERS Active Colloids. *Appl Spectrosc* **1993,** *47*, 1959-1964.

121. Mafune, F.; Kohno, J.; Takeda, Y.; Kondow, T.; Sawabe, H., Structure and Stability of Silver Nanoparticles in Aqueous Solution Produced by Laser Ablation. *J Phys Chem B* **2000,** *104*, 8333-8337.

122. Dolgaev, S. I.; Simakin, A. V.; Voronov, V. V.; Shafeev, G. A.; Bozon-Verduraz, F., Nanoparticles Produced by Laser Ablation of Solids in Liquid Environment. *Appl Surf Sci* **2002,** *186*, 546-551.

123. Kabashin, A. V.; Meunier, M., Synthesis of Colloidal Nanoparticles During Femtosecond Laser Ablation of Gold in Water. *J Appl Phys* **2003,** *94*, 7941-7943.

124. Zhang, D. S.; Goekce, B.; Barcikowski, S., Laser Synthesis and Processing of Colloids: Fundamentals and Applications. *Chem Rev* **2017,** *117*, 3990-4103.

125. Svrcek, V.; Sasaki, T.; Shimizu, Y.; Koshizaki, N., Aggregation of Silicon Nanocrystals Prepared by Laser Ablation in Deionized Water. *J Laser Micro Nanoen* **2007,** *2*, 15-20.

126. Svrcek, V.; Sasaki, T.; Shimizu, Y.; Koshizaki, N., Blue Luminescent Silicon Nanocrystals Prepared by ns Pulsed Laser Ablation in Water. *Appl Phys Lett* **2006,** *89*, 213113.

127. Svrcek, V.; Mariotti, D.; Kondo, M., Ambient-Stable Blue Luminescent Silicon Nanocrystals Prepared by Nanosecond-Pulsed Laser Ablation in Water. *Opt Express* **2009,** *17*, 520-527.

128. Rioux, D.; Laferriere, M.; Douplik, A.; Shah, D.; Lilge, L.; Kabashin, A. V.; Meunier, M. M., Silicon Nanoparticles Produced by Femtosecond Laser Ablation in Water as Novel Contamination-Free Photosensitizers. *J Biomed Opt* **2009,** *14*, 021010.

129. Besner, S.; Kabashin, A. V.; Meunier, M., Fragmentation of Colloidal Nanoparticles by Femtosecond Laser-Induced Supercontinuum Generation. *Appl Phys Lett* **2006,** *89*, 233122.

130. Besner, S.; Kabashin, A. V.; Meunier, M., Two-Step Femtosecond Laser Ablation-Based Method for the Synthesis of Stable and Ultra-Pure Gold Nanoparticles in Water. *Appl Phys A-Mater* **2007,** *88*, 269-272.

131. Blandin, P.; Maximova, K. A.; Gongalsky, M. B.; Sanchez-Royo, J. F.; Chirvony, V. S.; Sentis, M.; Timoshenko, V. Y.; Kabashin, A. V., Femtosecond Laser Fragmentation from Water-Dispersed Microcolloids: Toward Fast Controllable Growth of Ultrapure Si-Based Nanomaterials for Biological Applications. *J Mater Chem B* **2013,** *1*, 2489-2495.

132. Al-Kattan, A.; Ryabchikov, Y. V.; Baati, T.; Chirvony, V.; Sachez-Royo, J. F.; Sentis, M.; Braguer, D.; Timoshenko, V. Y.; Esteve, M. A.; Kabashin, A. V., Ultrapure Laser-Synthesized Si Nanoparticles with Variable Oxidation States for Biomedical Applications. *J Mater Chem B* **2016,** *4*, 7852-7858.

133. Li, X. Y.; Pyatenko, A.; Shimizu, Y.; Wang, H. Q.; Koga, K.; Koshizaki, N., Fabrication of Crystalline Silicon Spheres by Selective Laser Heating in Liquid Medium. *Langmuir* **2011,** *27*, 5076-5080.

134. Ryabchikov, Y. V.; Popov, A. A.; Sentis, M.; Timoshenko, V. Y.; Kabashin, A. V. In *Structural Properties of Gold-Silicon Nanohybrids Formed by Femtosecond Laser Ablation in Water at Different Fluences*, SPIE LASE, SPIE: 2016; p 6.

135. Kögler, M.; Ryabchikov, Y. V.; Uusitalo, S.; Popov, A.; Popov, A.; Tselikov, G.; Välimaa, A.-L.; Al-Kattan, A.; Hiltunen, J.; Laitinen, R.; Neubauer, P.; Meglinski, I.; Kabashin, A. V., Bare Laser-Synthesized Au-Based Nanoparticles as Nondisturbing Surface-Enhanced Raman Scattering Probes for Bacteria Identification. *J Biophotonics* **2018,** *11*, e201700225.

136. Intartaglia, R.; Bagga, K.; Brandi, F.; Das, G.; Genovese, A.; Di Fabrizio, E.; Diaspro, A., Optical Properties of Femtosecond Laser-Synthesized Silicon Nanoparticles in Deionized Water. *J Phys Chem C* **2011,** *115*, 5102-5107.

137. Rodio, M.; Brescia, R.; Diaspro, A.; Intartaglia, R., Direct Surface Modification of Ligand-Free Silicon Quantum Dots Prepared by Femtosecond Laser Ablation in Deionized Water. *J Colloid Interf Sci* **2016,** *465*, 242-248.

138. Svrcek, V.; Mariotti, D.; Cvelbar, U.; Filipic, G.; Lozac'h, M.; McDonald, C.; Tayagaki, T.; Matsubara, K., Environmentally Friendly Processing Technology for Engineering Silicon Nanocrystals in Water with Laser Pulses. *J Phys Chem C* **2016,** *120*, 18822-18830.

139. Saitow, K., Silicon Nanoclusters Selectively Generated by Laser Ablation in Supercritical Fluid. *J Phys Chem B* **2005,** *109*, 3731-3733.

140. Saitow, K.; Yamamura, T., Effective Cooling Generates Efficient Emission: Blue, Green, and Red Light-Emitting Si Nanocrystals. *J Phys Chem C* **2009,** *113*, 8465-8470.

141. Wei, S. Y.; Yamamura, T.; Kajiya, D.; Saitow, K., White-Light-Emitting Silicon Nanocrystal Generated by Pulsed Laser Ablation in Supercritical Fluid: Investigation of Spectral Components as a Function of Excitation Wavelengths and Aging Time. *J Phys Chem C* **2012,** *116*, 3928-3934.

142. Intartaglia, R.; Barchanski, A.; Bagga, K.; Genovese, A.; Das, G.; Wagener, P.; Di Fabrizio, E.; Diaspro, A.; Brandi, F.; Barcikowski, S., Bioconjugated Silicon Quantum Dots from One-Step Green Synthesis. *Nanoscale* **2012,** *4*, 1271-1274.

143. Li, X. G.; He, Y. Q.; Talukdar, S. S.; Swihart, M. T., Process for Preparing Macroscopic Quantities of Brightly Photoluminescent Silicon Nanoparticles with Emission Spanning the Visible Spectrum. *Langmuir* **2003,** *19*, 8490-8496.

144. Sato, S.; Swihart, M. T., Propionic-Acid-Terminated Silicon Nanoparticles: Synthesis and Optical Characterization. *Chem Mater* **2006,** *18*, 4083-4088.

145. Erogbogbo, F.; Tien, C. A.; Chang, C. W.; Yong, K. T.; Law, W. C.; Ding, H.; Roy, I.; Swihart, M. T.; Prasad, P. N., Bioconjugation of Luminescent Silicon Quantum Dots for Selective Uptake by Cancer Cells. *Bioconjugate Chem* **2011,** *22*, 1081-1088.

146. May, J. L.; Erogbogbo, F.; Yong, K.-T.; Ding, H.; Law, W.-C.; Swihart, M. T.; Prasad, P. N., Enhancing Silicon Quantum Dot Uptake by Pancreatic Cancer Cells *Via* Pluronic® Encapsulation and Antibody Targeting. *J Solid Tumors* **2012,** *2*, 24-37.

147. Erogbogbo, F.; May, J.; Swihart, M.; Prasad, P. N.; Smart, K.; El Jack, S.; Korcyk, D.; Webster, M.; Stewart, R.; Zeng, I.; Jullig, M.; Bakeev, K.; Jamieson, M.; Kasabov, N.; Gopalan, B.; Liang, L.; Hu, R.; Schliebs, S.; Villas-Boas, S.; Gladding, P., Bioengineering Silicon Quantum Dot Theranostics Using a Network Analysis of Metabolomic and Proteomic Data in Cardiac Ischemia. *Theranostics* **2013,** *3*, 719-728.

148. Erogbogbo, F.; Liu, X.; May, J. L.; Narain, A.; Gladding, P.; Swihart, M. T.; Prasad, P. N., Plasmonic Gold and Luminescent Silicon Nanoplatforms for Multimode Imaging of Cancer Cells. *Integr Biol* **2013,** *5*, 144-150.

149. Erogbogbo, F.; Yong, K. T.; Hu, R.; Law, W. C.; Ding, H.; Chang, C. W.; Prasad, P. N.; Swihart, M. T., Biocompatible Magnetofluorescent Probes: Luminescent Silicon Quantum Dots Coupled with Superparamagnetic Iron(III) Oxide. *ACS Nano* **2010,** *4*, 5131-5138.

150. Erogbogbo, F.; Yong, K. T.; Roy, I.; Hu, R.; Law, W. C.; Zhao, W. W.; Ding, H.; Wu, F.; Kumar, R.; Swihart, M. T.; Prasad, P. N., *In Vivo* Targeted Cancer Imaging, Sentinel Lymph Node Mapping and Multi-Channel Imaging with Biocompatible Silicon Nanocrystals. *ACS Nano* **2011,** *5*, 413-423.

151. Lin, T.; Liu, X.; Zhou, B.; Zhan, Z. Y.; Cartwright, A. N.; Swihart, M. T., A Solution-Processed UV-Sensitive Photodiode Produced Using a New Silicon Nanocrystal Ink. *Adv Funct Mater* **2014,** *24*, 6016-6022.

152. Kim, S.; Lee, J. H.; Swihart, M. T.; Lee, J. C.; Kim, J. Y., Silicon Nanoparticle Size-Dependent Open Circuit Voltage in an Organic-Inorganic Hybrid Solar Cell. *Curr Appl Phys* **2014,** *14*, 127-131.

153. Kim, S.; Jeon, K.; Lee, J. C.; Swihart, M. T.; Yang, M., Enhanced Performance of a Polymer Solar Cell Upon Addition of Free-Standing, Freshly Etched, Photoluminescent Silicon Nanocrystals. *Appl Phys Express* **2012,** *5*, 022302.

154. Alkis, S.; Oruc, F. B.; Ortac, B.; Kosger, A. C.; Okyay, A. K., A Plasmonic Enhanced Photodetector Based on Silicon Nanocrystals Obtained through Laser Ablation. *J Optics* **2012,** *14*, 125001.

155. Wu, M. H.; Mu, R.; Ueda, A.; Henderson, D. O.; Vlahovic, B., Production of Silicon Quantum Dots for Photovoltaic Applications by Picosecond Pulsed Laser Ablation. *Mat Sci Eng B-Solid* **2005,** *116*, 273-277.

156. Maier-Flaig, F.; Rinck, J.; Stephan, M.; Bocksrocker, T.; Bruns, M.; Kubel, C.; Powell, A. K.; Ozin, G. A.; Lemmer, U., Multicolor Silicon Light-Emitting Diodes (SiLEDs). *Nano Lett* **2013,** *13*, 475-480.

157. Puzzo, D. P.; Henderson, E. J.; Helander, M. G.; Wang, Z. B.; Ozin, G. A.; Lu, Z. H., Visible Colloidal Nanocrystal Silicon Light-Emitting Diode. *Nano Lett* **2011,** *11*, 1585-1590.

158. Cheng, K. Y.; Anthony, R.; Kortshagen, U. R.; Holmes, R. J., High-Efficiency Silicon Nanocrystal Light-Emitting Devices. *Nano Lett* **2011,** *11*, 1952-1956.

159. Angı, A.; Loch, M.; Sinelnikov, R.; Veinot, J. G. C.; Becherer, M.; Lugli, P.; Rieger, B., The Influence of Surface Functionalization Methods on the Performance of Silicon Nanocrystal Leds. *Nanoscale* **2018,** *10*, 10337-10342.

160. Meinardi, F.; Ehrenberg, S.; Dhamo, L.; Carulli, F.; Mauri, M.; Bruni, F.; Simonutti, R.; Kortshagen, U.; Brovelli, S., Highly Efficient Luminescent Solar Concentrators Based on Earth-Abundant Indirect-Bandgap Silicon Quantum Dots. *Nat Photonics* **2017,** *11*, 177-185.

161. Kim, S.; Hwang, C.; Park, S. Y.; Ko, S. J.; Park, H.; Choi, W. C.; Kim, J. B.; Kim, D. S.; Park, S.; Kim, J. Y.; Song, H. K., High-Yield Synthesis of Single-Crystal Silicon Nanoparticles as Anode Materials of Lithium Ion Batteries *Via* Photosensitizer-Assisted Laser Pyrolysis. *J Mater Chem A* **2014,** *2*, 18070-18075.

162. Aghajamali, M.; Xie, H.; Javadi, M.; Kalisvaart, W. P.; Buriak, J. M.; Veinot, J. G. C., Size and Surface Effects of Silicon Nanocrystals in Graphene Aerogel Composite Anodes for Lithium Ion Batteries. *Chem Mater* **2018,** *30*, 7782-7792.

163. Antoniadis, H.; Jiang, F.; Shan, W.; Liu, Y. In *All Screen Printed Mass Produced Silicon Ink Selective Emitter Solar Cells*, 2010 35th IEEE Photovoltaic Specialists Conference, 20-25 June 2010; 2010; pp 001193-001196.

164. Govoni, M.; Marri, I.; Ossicini, S., Carrier Multiplication between Interacting Nanocrystals for Fostering Silicon-Based Photovoltaics. *Nat Photonics* **2012,** *6*, 672-679.

165. Stupca, M.; Alsalhi, M.; Saud, T. A.; Almuhanna, A.; Nayfeh, M. H., Enhancement of Polycrystalline Silicon Solar Cells Using Ultrathin Films of Silicon Nanoparticle. *Appl Phys Lett* **2007,** *91*, 063107.

166. Rasouli, H. R.; Ghobadi, A.; Ghobadi, T. G. U.; Ates, H.; Topalli, K.; Okyay, A. K., Nanosecond Pulsed Laser Ablated Sub-10 Nm Silicon Nanoparticles for Improving Photovoltaic Conversion Efficiency of Commercial Solar Cells. *J Optics* **2017,** *19*, 105902.

167. Pi, X.; Zhang, L.; Yang, D., Enhancing the Efficiency of Multicrystalline Silicon Solar Cells by the Inkjet Printing of Silicon-Quantum-Dot Ink. *J. Phys Chem C* **2012,** *116*, 21240-21243.

168. Yu, T.; Wang, F.; Xu, Y.; Ma, L.; Pi, X.; Yang, D., Graphene Coupled with Silicon Quantum Dots for High-Performance Bulk-Silicon-Based Schottky-Junction Photodetectors. *Adv Mater* **2016,** *28*, 4912-4919.

169. Alsari, M.; Omar, Y. M.; Panda, M. K.; Chiesa, M.; Naumov, P.; Lilliu, S., Detrimental Effect of Silicon Nanoparticles on P3HT:PCBM-Based OPV Devices. *Macromol Chem Phys* **2015,** *216*, 1155-1160.

170. Ryu, J.; Hong, D.; Lee, H.-W.; Park, S., Practical Considerations of Si-Based Anodes for Lithium-Ion Battery Applications. *Nano Res* **2017,** *10*, 3970-4002.

171. Mihailescu, I. N.; Caricato, A. P., *Pulsed Laser Ablation: Advances and Applications in Nanoparticles and Nanostructuring Thin Films*. Pan Stanford: Milton, 2018, 499-523.

172. Radhakrishnan, G.; Adams, P. M.; Foran, B.; Quinzio, M. V.; Brodie, M. J., Pulsed Laser Deposited Si on Multilayer Graphene as Anode Material for Lithium Ion Batteries. *APL Materials* **2013,** *1*, 062103.

173. Biserni, E.; Xie, M.; Brescia, R.; Scarpellini, A.; Hashempour, M.; Movahed, P.; George, S. M.; Bestetti, M.; Li Bassi, A.; Bruno, P., Silicon Algae with Carbon Topping as Thin-Film Anodes for Lithium-Ion Microbatteries by a Two-Step Facile Method. *J Power Sources* **2015,** *274*, 252-259.

174. Garino, N.; Biserni, E.; Bassi, A. L.; Bruno, P.; Gerbaldi, C., Mesoporous Si and Multi-Layered Si/C Films by Pulsed Laser Deposition as Li-Ion Microbattery Anodes. *J Electrochem Soc* **2015,** *162*, A1816-A1822.

175. Bunker, C. E.; Smith, M. J., Nanoparticles for Hydrogen Generation. *J Mater Chem* **2011,** *21*, 12173-12180.

176. Rohani, P.; Kim, S.; Swihart, M. T., Boron Nanoparticles for Room-Temperature Hydrogen Generation from Water. *Adv Energy Mater* **2016,** *6*, 1502550.

177. Kobayashi, Y.; Matsuda, S.; Imamura, K.; Kobayashi, H., Hydrogen Generation by Reaction of Si Nanopowder with Neutral Water. *J Nanoparticle Res* **2017,** *19*, 176.

178. Xu, L.; Ashraf, S.; Hu, J.; Edwards, P. P.; Jones, M. O.; Hadzifejzovic, E.; Foord, J. S., Ball-Milled Si Powder for the Production of H_2 from Water for Fuel Cell Applications. *Int J Hydrogen Energ* **2016,** *41*, 12730-12737.

179. Brack, P.; Chillman, M.; Wijayantha, K. G. U.; Adcock, P.; Foster, S.; Dann, S. E., Activation of Silicon Towards Hydrogen Generation by Pelletisation. *J Alloys Compd* **2017,** *704*, 146-151.

180. Brack, P.; Dann, S. E.; Wijayantha, K. G. U.; Adcock, P.; Foster, S., An Assessment of the Viability of Hydrogen Generation from the Reaction of Silicon Powder and Sodium Hydroxide Solution for Portable Applications. *Int J Energy Res* **2017,** *41*, 220-228.

181. Xie, G. P.; Sun, J.; Zhong, G. R.; Shi, L. Y.; Zhang, D. W., Biodistribution and Toxicity of Intravenously Administered Silica Nanoparticles in Mice. *Arch Toxicol* **2010,** *84*, 183-190.

182. Liu, J. W.; Erogbogbo, F.; Yong, K. T.; Ye, L.; Liu, J.; Hu, R.; Chen, H. Y.; Hu, Y. Z.; Yang, Y.; Yang, J. H.; Roy, I.; Karker, N. A.; Swihart, M. T.; Prasad, P. N., Assessing Clinical Prospects of Silicon Quantum Dots: Studies in Mice and Monkeys. *ACS Nano* **2013,** *7*, 7303-7310.

183. Song, J. H.; Sailor, M. J., Quenching of Photoluminescence from Porous Silicon by Aromatic Molecules. *J Am Chem Soc* **1997,** *119*, 7381-7385.

184. Li, S.; Germanenko, I. N.; El-Shall, M. S., Semiconductor Nanoparticles in Contact: Quenching of the Photoluminescence from Silicon Nanocrystals by WO_3 Nanoparticles Suspended in Solution. *J Phys Chem B* **1998,** *102*, 7319-7322.

185. Germanenko, I. N.; Li, S.; El-Shall, M. S., Decay Dynamics and Quenching of Photoluminescence from Silicon Nanocrystals by Aromatic Nitro Compounds. *J Phys Chem B* **2001,** *105*, 59-66.

186. Patskovsky, S.; Bah, S.; Meunier, M.; Kabashin, A. V., Characterization of High Refractive Index Semiconductor Films by Surface Plasmon Resonance. *Appl Optics* **2006,** *45*, 6640-6645.

187. Patskovsky, S.; Kabashin, A. V.; Meunier, M.; Luong, J. H. T., Silicon-Based Surface Plasmon Resonance Sensing with Two Surface Plasmon Polariton Modes. *Appl Optics* **2003,** *42*, 6905-6909.

188. Warner, J. H.; Hoshino, A.; Yamamoto, K.; Tilley, R. D., Water-Soluble Photoluminescent Silicon Quantum Dots. *Angew Chem, Int Edit* **2005,** *44*, 4550-4554.

189. Li, Z. F.; Ruckenstein, E., Water-Soluble Poly(Acrylic Acid) Grafted Luminescent Silicon Nanoparticles and Their Use as Fluorescent Biological Staining Labels. *Nano Lett* **2004,** *4*, 1463-1467.

190. Whaley, S. R.; English, D. S.; Hu, E. L.; Barbara, P. F.; Belcher, A. M., Selection of Peptides with Semiconductor Binding Specificity for Directed Nanocrystal Assembly. *Nature* **2000,** *405*, 665-668.

191. Slocik, J. M.; Moore, J. T.; Wright, D. W., Monoclonal Antibody Recognition of Histidine-Rich Peptide Encapsulated Nanoclusters. *Nano Lett* **2002,** *2*, 169-173.

192. Djalali, R.; Chen, Y. F.; Matsui, H., Au Nanocrystal Growth on Nanotubes Controlled by Conformations and Charges of Sequenced Peptide Templates. *J Am Chem Soc* **2003,** *125*, 5873-5879.

193. Zhang, X.; Brynda, M.; Britt, R. D.; Carroll, E. C.; Larsen, D. S.; Louie, A. Y.; Kauzlarich, S. M., Synthesis and Characterization of Manganese-Doped Silicon Nanoparticles: Bifunctional Paramagnetic-Optical Nanomaterial. *J Am Chem Soc* **2007,** *129*, 10668-10669.

194. Bull, S. R.; Guler, M. O.; Bras, R. E.; Meade, T. J.; Stupp, S. I., Self-Assembled Peptide Amphiphile Nanofibers Conjugated to MRI Contrast Agents. *Nano Lett* **2005,** *5*, 1-4.

195. Yang, H. S.; Santra, S.; Walter, G. A.; Holloway, P. H., Gd^{III}-Functionalized Fluorescent Quantum Dots as Multimodal Imaging Probes. *Adv Mater* **2006,** *18*, 2890-2894.

196. Tan, W. B.; Zhang, Y., Multifunctional Quantum-Dot-Based Magnetic Chitosan Nanobeads. *Adv Mater* **2005,** *17*, 2375-2380.

197. Aptekar, J. W.; Cassidy, M. C.; Johnson, A. C.; Barton, R. A.; Lee, M.; Ogier, A. C.; Vo, C.; Anahtar, M. N.; Ren, Y.; Bhatia, S. N.; Ramanathan, C.; Cory, D. G.; Hill, A. L.; Mair, R. W.; Rosen, M. S.; Walsworth, R. L.; Marcus, C. M., Silicon Nanoparticles as Hyperpolarized Magnetic Resonance Imaging Agents. *ACS Nano* **2009,** *3*, 4003-4008.

198. Tu, C. Q.; Ma, X. C.; Pantazis, P.; Kauzlarich, S. M.; Louie, A. Y., Paramagnetic, Silicon Quantum Dots for Magnetic Resonance and Two-Photon Imaging of Macrophages. *J Am Chem Soc* **2010,** *132*, 2016-2023.

199. Erogbogbo, F.; Chang, C.-W.; May, J. L.; Liu, L.; Kumar, R.; Law, W.-C.; Ding, H.; Yong, K. T.; Roy, I.; Sheshadri, M.; Swihart, M. T.; Prasad, P. N., Bioconjugation of Luminescent Silicon Quantum Dots to Gadolinium Ions for Bioimaging Applications. *Nanoscale* **2012,** *4*, 5483-5489.

200. Uusitalo, S.; Popov, A.; Ryabchikov, Y. V.; Bibikova, O.; Alakomi, H.-L.; Juvonen, R.; Kontturi, V.; Siitonen, S.; Kabashin, A.; Meglinski, I.; Hiltunen, J.; Laitila, A., Surface-Enhanced Raman Spectroscopy for Identification and Discrimination of Beverage Spoilage Yeasts Using Patterned Substrates and Gold Nanoparticles. *J Food Engng* **2017,** *212*, 47-54.

201. Mirza, A. N.; Fornage, B. D.; Sneige, N.; Kuerer, H. M.; Newman, L. A.; Ames, F. C.; Singletary, S. E., Radiofrequency Ablation of Solid Tumors. *Cancer J* **2001,** *7*, 95-102.

202. Gannon, C. J.; Cherukuri, P.; Yakobson, B. I.; Cognet, L.; Kanzius, J. S.; Kittrell, C.; Weisman, R. B.; Pasquali, M.; Schmidt, H. K.; Smalley, R. E.; Curley, S. A., Carbon Nanotube-Enhanced Thermal Destruction of Cancer Cells in a Noninvasive Radiofrequency Field. *Cancer-Am Cancer Soc* **2007,** *110*, 2654-2665.

203. Moran, C. H.; Wainerdi, S. M.; Cherukuri, T. K.; Kittrell, C.; Wiley, B. J.; Nicholas, N. W.; Curley, S. A.; Kanzius, J. S.; Cherukuri, P., Size-Dependent Joule Heating of Gold Nanoparticles Using Capacitively Coupled Radiofrequency Fields. *Nano Res* **2009,** *2*, 400-405.

204. James, W. D.; Hirsch, L. R.; West, J. L.; O'Neal, P. D.; Payne, J. D., Application of INAA to the Build-Up and Clearance of Gold Nanoshells in Clinical Studies in Mice. *J Radioanal Nucl Ch* **2007,** *271*, 455-459.

205. Afshani, P.; Moussa, S.; Atkinson, G.; Kisurin, V. Y.; Samy El-Shall, M., Enhanced Photothermal Effect of Surface Oxidized Silicon Nanocrystals Anchored to Reduced Graphene Oxide Nanosheets. *Chem Phys Lett* **2016,** *650*, 148-153.

206. Kabashin, A. V.; Timoshenko, V. Y., What Theranostic Applications Could Ultrapure Laser-Synthesized Si Nanoparticles Have in Cancer? *Nanomedicine-Uk* **2016,** *11*, 2247-2250.

207. Rohani, P.; Banerjee, S.; Sharifi-Asl, S.; Malekzadeh, M.; Shahbazian-Yassar, R.; Billinge, S. J. L.; Swihart, M. T., Synthesis and Properties of Plasmonic Boron-Hyperdoped Silicon Nanoparticles. *Adv Funct Mater* **2019,** *29*, 1807788.

208. Mi, X.; Benito, M.; Putz, S.; Zajac, D. M.; Taylor, J. M.; Burkard, G.; Petta, J. R., A Coherent Spin–Photon Interface in Silicon. *Nature* **2018,** *555*, 599-603.

209. He, G. S.; Zheng, Q.; Yong, K.-T.; Erogbogbo, F.; Swihart, M. T.; Prasad, P. N., Two- and Three-Photon Absorption and Frequency Upconverted Emission of Silicon Quantum Dots. *Nano Lett* **2008,** *8*, 2688-2692.

210. Chandra, S.; Ghosh, B.; Beaune, G.; Nagarajan, U.; Yasui, T.; Nakamura, J.; Tsuruoka, T.; Baba, Y.; Shirahata, N.; Winnik, F. M., Functional Double-Shelled Silicon Nanocrystals for Two-Photon Fluorescence Cell Imaging: Spectral Evolution and Tuning. *Nanoscale* **2016,** *8*, 9009-9019.

211. Kharin, A. Y.; Lysenko, V. V.; Rogov, A.; Ryabchikov, Y. V.; Geloen, A.; Tishchenko, I.; Marty, O.; Sennikov, P. G.; Kornev, R. A.; Zavestovskaya, I. N.; Kabashin, A. V.; Timoshenko, V. Y., Bi-Modal Nonlinear Optical Contrast from Si Nanoparticles for Cancer Theranostics. *Adv Opt Mater* **2019,** *7*, 1801728.

212. Erogbogbo, F.; Liu, T.; Ramadurai, N.; Tuccarione, P.; Lai, L.; Swihart, M. T.; Prasad, P. N., Creating Ligand-Free Silicon Germanium Alloy Nanocrystal Inks. *ACS Nano* **2011,** *5*, 7950-7959.

213. Kim, S.; Park, S. Y.; Jeong, J.; Kim, G.-H.; Rohani, P.; Kim, D. S.; Swihart, M.; Kim, J. Y., Production of Pristine, Sulfur-Coated and Silicon-Alloyed Germanium Nanoparticles *via* Laser Pyrolysis. *Nanotechnology* **2015,** *26*, 305703.

214. Petriev, V. M.; Tischenko, V. K.; Mikhailovskaya, A. A.; Popov, A. A.; Tselikov, G.; Zelepukin, I.; Deyev, S. M.; Kaprin, A. D.; Ivanov, S.; Timoshenko, V. Y.; Prasad, P. N.; Zavestovskaya, I. N.; Kabashin, A. V., Nuclear Nanomedicine Using Si Nanoparticles as Safe and Effective Carriers of ^{188}Re Radionuclide for Cancer Therapy. *Sci Rep* **2019,** *9*, 2017.

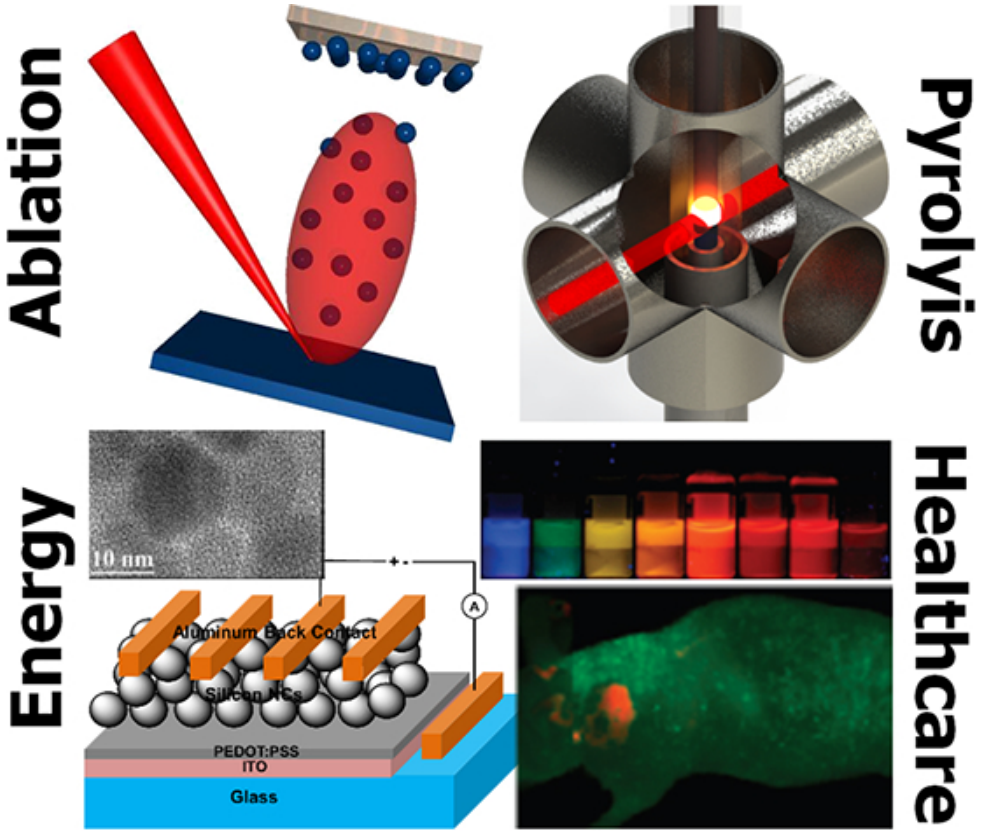

TOC image

48x39mm (300 x 300 DPI)